MAGNETIC SPECTRA OF THE DIMER O_2AR

JACOB METTES

MAGNETIC SPECTRA OF THE DIMER O_2AR

Though this be madness,
yet there is method in't.

PROMOTORES: PROF. DR. J. REUSS
PROF. DR. IR. A. VAN DER AVOIRD

CO-REFERENT: DR. D. C. LAINÉ

MAGNETIC SPECTRA OF THE DIMER O_2AR

PROEFSCHRIFT

TER VERKRIJGING VAN DE GRAAD VAN DOCTOR
IN DE WISKUNDE EN NATUURWETENSCHAPPEN
AAN DE KATHOLIEKE UNIVERSITEIT TE NIJMEGEN,
OP GEZAG VAN DE RECTOR MAGNIFICUS
PROF. DR. J. H. G. I. GIESBERS
VOLGENS BESLUIT VAN HET COLLEGE VAN DEKANEN
IN HET OPENBAAR TE VERDEDIGEN
OP VRIJDAG 4 MEI 1984
DES NAMIDDAGS TE 2.00 UUR PRECIES

door

JACOB METTES

geboren te Nijmegen

DRUKKERIJ VAN MAMEREN B.V., NIJMEGEN

Velen hebben bijgedragen aan de tot standkoming van dit proefschrift. In het bijzonder wil ik bedanken

J. Holtkamp voor de "computer controllable" machine.

D. Lainé voor de microgolf cavities en zijn regelmatige werkbezoeken.

J. Tennyson voor zijn geweldige berekeningen en de fijne samenwerking.

F. Van Rijn voor het particle counting systeem.

H. Clephas, B. Heijmen en P. Verhoeve voor de medewerking tijdens hun afstudeerperiode.

C. Sikkens en L. Hendriks voor hun technische en tekenkundige hulp.

G. Brocks voor zijn "last minute" berekeningen.

L. Meerts voor de EBR excursie.

Alle dienstverlenende afdelingen van de faculteit wiskunde en natuurwetenschappen.

Het onderzoek dat in dit proefschrift beschreven staat, is een gedeelte van het onderzoeksprogramma van de "Stichting voor Fundamenteel Onderzoek der Materie" (FOM), welke financieel gesteund wordt door de "Nederlandse Organisatie voor Zuiver Wetenschappelijk Onderzoek" (ZWO).

Tenslotte de NATO voor het verschaffen van een "travel grant" voor Derek Lainé.

aan Marline

CONTENTS

PAPER III; Method to determine the rotational temperature in a molecular beam, demonstrated on O_2

PAPER IV; Magnetic spectra of the dimer O_2Ar

This thesis contains four separate papers;

I, a computer study on the system O_2-Ar published with Tennyson in Chem. Phys. 76(1983) 195,

II, an analysis of the properties of this system, based on a T-shaped model for the complex; a paper published by Van der Avoird in J. Chem. Phys. 79(1983) 1170,

III, an experimental investigation, of the thermal distribution of O_2-molecules expanding in a supersonic molecular beam, performed together with Heijmen, Lainé and Reuss, accepted for publication in Chem Phys.;

IV, a study of Zeeman-transitions of O_2-Ar with the magnetic beam resonance technique machine, to be published and co-authored by Heijmen, Verhoeve, Laine and Reuss.

Part II has thus not grown in my own garden, but in my neighbourhood. It forms such an essential part of the total effort presented in this thesis that it simply had to be included.

The total effort was directed towards understanding the dynamics of O_2-Ar, a complex known to be semi-rigid. One must admit, however, that large amplitude motions are present, for all Van der Waals complexes; the angle of the T-shape structure of our O_2-Ar, which is 90 degrees on the average, is subject to variations of about 30 degrees. Nevertheless, there are floppier complexes, e.g. H_2-Ne which has been studied experimentally and theoretically before, in our laboratory.

The constraints formed by the T-shape have been beautifully translated into an appropriate choice of first order basic functions, see II. This opened the way to a proper physical understanding of what goes on in a loosely bound complex with constraints.

We were lucky to find an experimental approach to the dynamical properties of O_2-Ar, i.e. the Zeeman splitting in weak magnetic field (IV). The experimental accuracy (about 50 KHz) was matched to the observable spectral structure of this phenomenon.

It was a tedious enterprise to achieve high detection efficiency and noise suppresssion in order to render the tiny fraction of 10^{-5} of O_2Ar complexes of the total of the O_2 signal, significant for this spectroscopic study. This fraction, moreover, is distributed over many states further diluting the relevant signals.

On our way we learned to tame molecular beams; as one of the results we found an alternative way to determine molecular beam temperatures (III) which guided us during the final battle to obtain cold complexes (about 3K).

If one reconsiders all those hours during which the molecular beam apparatus has been dis- and reassembled, to run finally for two months under computer control day and night, -all the hours spend on the theory and the computer programs leading to the numerical and analytical approach described below- what was achieved quantitatively? We claim to know now one piece of the repulsive branch of the angle dependent part for the O_2-Ar potential around R = 3.7 Å.

Comparing this knowledge with predictions by the Perugia group, little progress seems to have been achieved, indeed; 0.05 Å to be precise! However, what we know now for sure, was a fortunate guess before. The slight shift of 0.05 Å (see IV fig. 5 below) does not measure the progress in knowledge, really.

Calculated ro-vibrational fine structure spectrum and weak-field Zeeman splittings of the O_2Ar Van der Waals molecule

Jonathan Tennyson*
Instituut voor Theoretische Chemie
Katholieke Universiteit
Toernooiveld
6525 ED Nijmegen
The Netherlands

and

Jacques Mettes
Fysisch Laboratorium
Katholieke Universiteit
Toernooiveld
6525 ED Nijmegen
The Netherlands

* Present address: SERC Daresbury Laboratory,
Daresbury, Warrington, Cheshire,
WA4 4AD, U.K.

Abstract

Ro-vibrational calculations are performed on O_2Ar explicitly including coupling to the O_2 electronic spin. Two different empirical potentials are used and give similar fine structure spectra. The anisotropy in the potential is found to strongly perturb the O_2 fine structure spectrum suggesting that the O_2Ar fine structure spectrum can give detailed information about the anisotropy of the Van der Waals interaction potential. Transition strengths for the complex fine structure transitions are calculated and found to vary by two orders of magnitude. The Zeeman splitting of the levels by interaction with a weak magnetic field is also calculated.

1. Introduction

There has been much recent interest, both theoretical and experimental, in Van der Waals molecules [1]. The study of the dynamics these loosely bound complexes has led to the development of special techniques capable of representing large ro-vibrational modes in one or more dimensions [2-7]. Given a potential energy surface for a system, these methods can give accurate predictions of ro-vibrational spectra.

Recently, Reuss and co-workers [8,9] have measured the hyperfine spectrum of H_2-X (X = Noble gas, H_2) Van der Waals molecules. By use of a vector model [10], they were able to invert this data to obtain accurate information about the Van der Waals potential in the bonding region. In particular their data probed the leading anisotropic term, $V_2(R)$, to which other experiments are often less sensitive. The vector model, which treats L, the end-over-end rotation of the complex, as a good quantum number is appropriate to H_2 complexes because of the large splitting ($\sim$ 350 cm^{-1}) between the H_2 rotational states. This allows the coupling between rotational states to be neglected to a very good approximation [5].

Oxygen is an interesting species because of its paramagnetic electronic ground state. Coupling to this $^3\Sigma_g^-$ state leads to the characteristic fine structure of O_2 ro-vibrational states; fine structure transitions lie largely in the 60 GHz region [11]. These levels are further split in a magnetic field by Zeeman interaction [12]. ^{16}O has zero nuclear spin meaning that there is no nuclear hyperfine interaction; Bose-Einstein statistics forbids even rotational states in the $^3\Sigma_g^-$ ground state.

The ro-vibrational states of Van der Waals complexes of O_2 will also be split by spin-orbit interactions. Observation of these splittings could yield valuable information about the Van der Waals interaction potential. However, the small splitting between O_2 rotational states ($\sim$ 2.8 cm^{-1}) means that rotational states can be strongly coupled in the dimer, making the use of the vector model

inappropriate.

Two empirically motivated interaction potentials for the O_2Ar Van der Waals dimer are available [13,14]. Both are expressed as Legendre expansions in cosθ

$$V(R,\theta) = \sum_{\lambda} V_{\lambda}(R)\ P_{\lambda}(\cos\theta) \qquad (1)$$

truncated at $\lambda = 2$; only λ even contributes by symmetry. R and θ are defined in Fig. 1. Mingelgrin and Gordon's $V_{\lambda}(R)$'s have a R^{-6}-exponential form [13], whereas those of Pirani and Vecchiocattivi are based on a more sophisticated fit to a variety of experimental data [14].

In this work we use these potentials to calculate the low temperature fine-structure spectrum for O_2-Ar. We used a method capable of giving all the ro-vibrational states of the complex and a coupling scheme analogous to that of the vector model [10]. This approach uses no approximate quantum numbers. From these levels we obtain Boltzmann distributions for several temperatures. With these distributions and the relevant transition dipole moments one can make predictions of the signal to noise ratio of the dimer transitions relative to pure O_2. These ratios are important if the fine structure of the O_2Ar complex is to be observed. Our calculations also allow us to assess what information could be expected from such an experiment and in what region one would expect to see transitions. Finally, we also consider how the low-lying levels of the complex are split by interaction with a weak magnetic field.

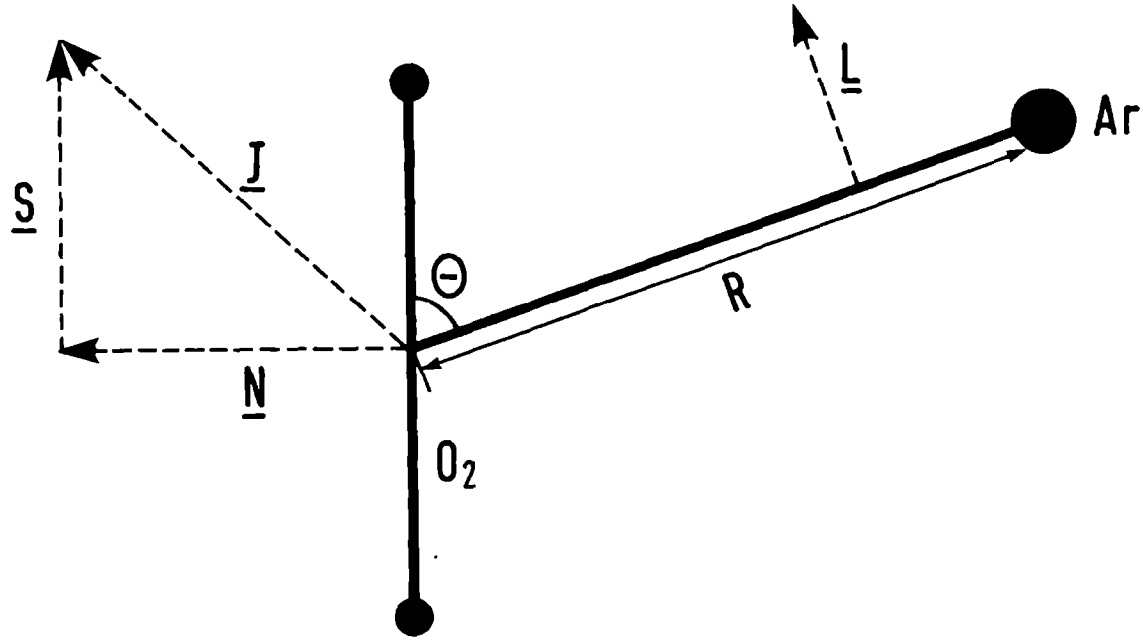

Fig. 1: Coupling scheme used for the O_2Ar calculations ((NS)JL)F, where the angular momentum vectors are defined in the text.

2. Method

In the absence of a magnetic field the Hamiltonian for the problem can be written

$$\hat{\underline{H}} = \hat{\underline{H}}_{VR} + \hat{\underline{H}}_{Fine} \tag{2}$$

$\hat{\underline{H}}_{VR}$ is the usual space-fixed vibration-rotation Hamiltonian for the interaction of an atom with a rigid diatom [2]

$$\hat{\underline{H}}_{VR} = \frac{-\hbar^2}{2\mu R}\left(\frac{\partial^2}{\partial R^2}\right) R + \frac{\hat{\underline{L}}^2}{2\mu R^2} + B_{O_2}\,\hat{\underline{N}}^2 + V(R,\theta) \tag{3}$$

where $\mu = m_a m_d/(m_a+m_d)$, with m_a and m_d being the atomic and diatomic masses respectively; B_{O_2} is the rotational constant of O_2, for which a value of 43.1005 GHz [15] was used. The eigenfunctions of the operators $\hat{\underline{L}}^2$ and $\hat{\underline{N}}^2$ are spherical harmonics $|LM_L\rangle$ and $|NM_N\rangle$ with eigenvalues L(L+1) and N(N+1).

$\hat{\underline{H}}_{Fine}$ consists of the terms which couple the O_2 electronic spin to the orbital motion. For this we have used the same Hamiltonian as is appropriate for pure O_2, for which Hund's rule case (b) applies [15]. Following Mizushima [15], $\hat{\underline{H}}_{Fine}$ comprises a spin orbit coupling term and a Coriolis term

$$\hat{\underline{H}}_{Fine} = \mu_0\,\hat{\underline{N}}\cdot\hat{\underline{S}} + \frac{2}{3}\lambda_0\,(3\hat{S}_\xi^2 - \hat{\underline{S}}^2) \tag{4}$$

where S_ξ is the projection of $\underline{S}$ on the O_2 bond axis. For $^{16}O_2$ $\mu_0 = -0.252585$ GHz and $\lambda_0 = 59.501342$ GHz [15]. The operators $\hat{S}_z^2$ and $\hat{\underline{S}}^2$ act on the spin functions $|SM_s\rangle$.

Following Waaijer et al.[10] angular basis functions were taken as coupled spherical harmonics in the form $|((NS)JL)FM_F\rangle$. $|NM_N\rangle$ represents the O_2 rotations, N must be odd, and $|SM_S\rangle$ the angular momentum of the spin, for the ground state

S = 1. These couple to $|JM_J\rangle$, where J and M_J are the total angular momentum quantum numbers of pure O_2 [15]. In the dimer $|JM_J\rangle$ couples with $|LM_L\rangle$, the end-over-end rotations of the complex, to give $|FM_F\rangle$. F, M_F and the parity $p = (-1)^{N+S+L+1}$ are the only good quantum numbers of the complex. Fig. 1 illustrates this coupling scheme. Previous [1,2] atom-diatom ro-vibrational calculations performed on S = 0 systems have used the simplified coupling scheme $|(NL)FM_F\rangle$.

To our angular basis set we added a set of radial functions generated numerically by explicit integration of the pseudo-diatomic problem obtained by considering N = 0, L = 0 and $V(R,\theta) = V_0(R)$, see ref. 7 for details. This gives a total basis set which can be written

$$\{\chi_q(R)\ |((NS)JL)F\ M_F\rangle;\ N,q\} \tag{5}$$

As with previous work [2,5-7], all possible functions with $q \leq q_{max}$ and $N \leq N_{max}$ were included in the basis.

Matrix elements over the radial operators in $\hat{\underline{H}}_{VR}$ were obtained by explicit numerical integration [2,7]. Matrix elements of the angular functions were obtained by use of the Wigner-Eckart theorem and successive decoupling of the resulting reduced matrix elements [16].

Writing $\langle i| = \langle((NS)JL)FM_F|$ and $|f\rangle = |((N'S)J'L')F'M_F'\rangle$ we obtain

$$\langle i|P_\lambda(\cos\theta)|f\rangle = \delta_{FF'}\,\delta_{M_F M_F'}\,(-1)^{F+S+J+J'}$$

$$[(2L+1)(2L'+1)(2N+1)(2N'+1)(2J+1)(2J'+1)]^{\frac{1}{2}} \begin{pmatrix} L & \lambda & L' \\ 0 & 0 & 0 \end{pmatrix}\begin{pmatrix} N & \lambda & N' \\ 0 & 0 & 0 \end{pmatrix}$$

$$\begin{Bmatrix} J & \lambda & J' \\ L' & F & L \end{Bmatrix}\begin{Bmatrix} N & \lambda & N' \\ J' & S & J \end{Bmatrix} \tag{6}$$

for the angular integral over the potential expressed in the form (1), where the 3-j and 6-j symbols are standard [17]. Writing S = 0 reduces this to the

more common Percival-Seaton coefficient [18].

As $\hat{H}_{Fine}$ contains only scalar operators, its matrix elements are unaffected by complex formation; they are [15]

$$\langle i|\hat{\underline{N}}\cdot\hat{\underline{S}}|f\rangle = \delta_{FF'}\,\delta_{M_F M_F'}\,\delta_{LL'}\,\delta_{NN'}\,\delta_{JJ'}\,(-1)^{N+S+J}$$

$$[S(S+1)(2S+1)\,N(N+1)(2N+1)]^{\frac{1}{2}} \begin{Bmatrix} N & S & J \\ S & N & 1 \end{Bmatrix} \qquad (7)$$

and

$$\langle i|(3\hat{S}_\xi^2-\hat{\underline{S}}^2)|f\rangle = \delta_{FF'}\,\delta_{M_F M_F'}\,\delta_{LL'}\,\delta_{JJ'}{}_L\,(-1)^{J+S}\,[30N(N+1)N'(N'+1)]^{\frac{1}{2}}$$

$$S(S+1)\,(2S+1) \begin{pmatrix} N & 2 & N' \\ 0 & 0 & 0 \end{pmatrix} \begin{Bmatrix} S & S & 1 \\ 2 & 1 & S \end{Bmatrix} \begin{Bmatrix} J & N' & S \\ 2 & S & N \end{Bmatrix} \qquad (8)$$

As in pure O_2, (7) is completely diagonal, but (8) mixes states differing by 2 in N. Both expressions can be simplified by use of the special values for 3-j and 6-j symbols [17], for example

$$\langle i|\hat{\underline{N}}\cdot\hat{\underline{S}}|f\rangle = \delta_{if}\,\tfrac{1}{2}[J(J+1) - S(S+1) - N(N+1)] \qquad (9)$$

With these matrix elements, a secular matrix for each F and p can be constructed and diagonalised giving the spin coupled ro-vibrational states for those quantum numbers.

No electric dipole transitions are possible in oxygen; however, the magnetic dipole moment of two Bohr magnetons allows magnetic dipole transitions. The perturbative Hamiltonian inducing these transitions is the same as the one which causes the first order Zeeman splitting of the levels in a weak-magnetic field [19]

$$\hat{\underline{H}}' = -g_e\,\mu_B\,\hat{\underline{S}}\cdot\underline{B} \qquad (10)$$

where μ_B is the Bohr magneton (1.39961 MHz/Gauss) and g_e is 2.00232 [15]. The transition intensity is thus proportional to $|\langle i|\hat{S}|f\rangle|^2$ and a Boltzmann factor which we discuss in section 4. Taking the z axis as the direction of $\underline{B}$, the relevant matrix element is

$$\langle i|\hat{S}_z|f\rangle = \delta_{M_F M_F'}\,\delta_{LL'}\,\delta_{NN'}\,(-1)^{L+S+N-M_F}$$

$$[(2F+1)(2F+3)(2J+1)(2J+3)S(S+1)(2S+1)]^{\frac{1}{2}} \begin{pmatrix} F & 1 & F' \\ -M_F & 0 & M_F' \end{pmatrix} \qquad (11)$$

$$\begin{Bmatrix} J & 1 & J' \\ F' & L & F \end{Bmatrix} \begin{Bmatrix} S & 1 & S \\ J' & N & J \end{Bmatrix}$$

which contains the selection rules $\Delta F = 0, \pm 1$ and $\Delta M_F = 0$. Eq. (11) is only non-zero for $|F-F'|$ and $|J-J'| \leq 1$ and reduces to the familiar form for O_2 [15,19] by substituting $L = 0$.

Again, $\langle i|\hat{S}_z|f\rangle$ can be written as five special cases by using the special values of the 3-j and 6-j symbols. We however will only comment on the M_F dependence of these. When $\Delta F = 0$, the matrix elements are all simply proportional to M_F. This causes the familiar first-order Zeeman levels which are equally spaced; see for example [12]. It also means that $\Delta F = 0$ transitions with $M_F = 0$ (e.g. $F = 0 \nleftrightarrow F' = 0$) are forbidden and those with $M_F = F$ are the most intense. For $F \rightarrow F+1$ transitions, all matrix elements are proportional to $((F+1) - M_F^2)^{\frac{1}{2}}$ which means that those with $M_F = 0$ are the most intense.

3. Calculated fine structure spectrum

A test calculation for $F = 0$ and p even showed that a basis set with $N \leq 7$ and $q \leq 4$ was well saturated. Increasing either N_{max} or q_{max} lowered none of the lowest five levels by more than 0.3 GHz; a test run with $F = 15$ gave the same result.

Calculations were thus performed with this basis for the potentials of Mingelgrin and Gordon (MG) [13] and Pirani and Vecchiocattivi (PV) [14] for F values up to 15. MG's potential was found to be considerably deeper than that of PV, the ground state ($F = 0$, p odd) lying at -3000.24 GHz compared with -2614.16 GHz. We,however, are interested in the fine structure transitions between low-lying states. Table 1 compares the transition frequencies of all the allowed transitions from the low lying states with $F \leq 2$.

In pure oxygen, the corresponding fine structure transitions are clustered in the region 56 - 62GHz with one transition at 118.75 GHz [11]. Our dimer calculations reproduce these transitions if the anisotropic term, V_2, in the potentials is switched off. The anisotropy in the potential is thus responsible for a drastic change in the fine structure spectrum upon complex formation. Inspection of the eigenvectors for the complex levels show the basis functions to be strongly mixed with no nearly good quantum numbers -unlike pure O_2 where N is nearly good or the vector model which assumes J and L to be good [10]. This suggests that an experimental observation of these fine structure transitions is capable of yielding sensitive information about the anisotropic potential of the Van der Waals complex.

Table 1 shows there to be a difference of nearly 400 GHz in the binding energies between the levels in the two potentials considered. Despite this,the calculated fine structure transitions are in good agreement, with differences often less than 1 GHz. This is more surprising when the anisotropy of the two potentials are compared (see Fig. 1, ref. [14]) as MG's potential is markedly more

anisotropic than that of PV in the region of the minimum of V_0. In contrast the (comparatively modest) reduction of PV's V_2 by one half perturbs the transitions by about 10%.

The transitions shown in Table 1 all arise from low-lying vibrational states. The anisotropy of both PV's and MG's potential cause these states to be predominantly localised about the perpendicular ($\theta = 90°$) geometry, in agreement with Henderson and Ewing's [20] analysis of their infrared spectrum. The similarity of these spatial distribution partially accounts for the similarity of the spectra.

As the potentials give similar results and that of PV can be regarded as more reliable, being fitted to the results of several experiments, we use this potential for the results presented in the remainder of this work.

Table 1 also gives the relative transition strengths for the transitions calculated using PV's potential. These numbers correspond to $\sum_{M_F} |\langle i|\hat{S}_z|j\rangle|^2$ and were thus calculated assuming all M_F levels to be degenerate. In practice, the earth's magnetic field may remove this degeneracy and different strengths for each M_F will be observed. These can be obtained from the values given in Table 1 by using the M_F dependence of $\langle i|\hat{S}_z|f\rangle$ given in the previous section.

The relative transition strengths presented in Table 1 vary by as much as a hundred between different transitions. This suggests that certain of the transitions listed are considerably more likely to be detectable than others.

Fig. 2 presents smoothed probability distributions as a function of temperatures. These were calculated by including all states with $F \leq 15$ which lay below -1500 GHz (77°K). This ensured that the normalising sum over the states was well converged. We note that "high temperature" O_2Ar spectra such as the one measured by Henderson and Ewing at 93°K sample a large number of ro-vibrational states making their quantitative analysis difficult. Also marked in Fig. 2 are the states which have the greatest population for each temperature.

Next we estimate the SNR (signal to noise ratio) of the dimer spectral lines compared to that of pure oxygen. The square of this relative SNR is proportional

to the ratio of the Boltzmann populations, the ratio of the transition strengths and machine dependent factors such as the relative population of dimer to pure O_2. Table 2 shows the partition functions, $Z = \sum_{\alpha,F} (2F+1) \exp(-E(\alpha,F)/kT)$, at several temperatures for O_2 and O_2Ar. Table 2 suggests that the partition function would cause a ten-fold reduction in intensity for an O_2Ar spectrum at 4°K compared to a pure O_2 spectrum at 15°K, realistic experimental temperatures. The transition strengths of the stronger dimer lines (those which do not couple strongly to $J = 0$) are similar to those of pure oxygen. For example, the O_2 $N = 1$, $J = 1 \rightarrow 2$ transition has a strength of 0.83 (compare with Table 1). The major reduction in relative signal to noise ratio will be caused by the smaller number of dimers, in for example a nozzle expansion, compared with pure O_2, and any lowering of machine sensitivity.

Table 1

Frequency and relative transition strengths of the allowed ($\Delta F = 0,\pm1$, parity conserved) fine structure transitions in O_2Ar for the low-lying states calculated using the potentials of Mingelgrin and Gordon (MG) [13] and Pirani and Vecchiocattivi (PV) [14]. The energies of the lower states relative to the dissociated Van der Waals complex are given for comparison.

F		parity	Transition frequency/GHz[a]		Transition strength	Energy/GHz[a]	
|i>	|f>		PV	MG	PV	PV	MG
2	3	e	11.44	11.89	0.418	-2562.78	-2948.69
2	2	o	39.59	39.34	0.022	-2602.36	-2988.01
1	2	e	47.44	47.47	0.012	-2610.22	-2996.16
2	3	o	50.14	51.12	0.379	-2602.36	-2988.01
2	1	e	52.87	54.46	0.949	-2562.78	-2948.69
2	2	e	58.37	59.80	0.362	-2562.78	-2948.69
2	3	e	74.97	77.41	0.049	-2562.78	-2948.69
2	2	e	76.01	77.29	0.041	-2562.78	-2948.69
2	1	o	91.20	92.32	0.014	-2602.36	-2988.01
1	1	e	100.31	101.94	0.488	-2610.22	-2996.16
2	2	o	101.35	102.98	0.805	-2602.36	-2988.01
0	1	o	103.00	104.55	0.515	-2614.16	-3000.24
2	1	o	105.33	105.78	0.877	-2602.36	-2988.01
1	2	e	105.81	107.27	0.946	-2610.22	-2996.16
1	0	e	107.88	108.22	0.357	-2610.22	-2996.16
2	3	o	108.57	109.99	1.366	-2602.36	-2988.01
0	1	o	117.13	118.01	0.145	-2614.16	-3000.24
1	2	e	123.45	124.76	0.174	-2610.22	-2996.16
2	3	o	130.44	132.19	0.096	-2602.36	-2988.01

[a] $1\ cm^{-1} = 29.97925$ GHz

Table 2

Partition function Z of O_2 and O_2Ar at different temperatures:

	2K	4K	6K	8K	10K	15K
O_2	2.3	4.2	5.6	7.1	8.3	11.9
O_2Ar	40	128	244	385	526	-

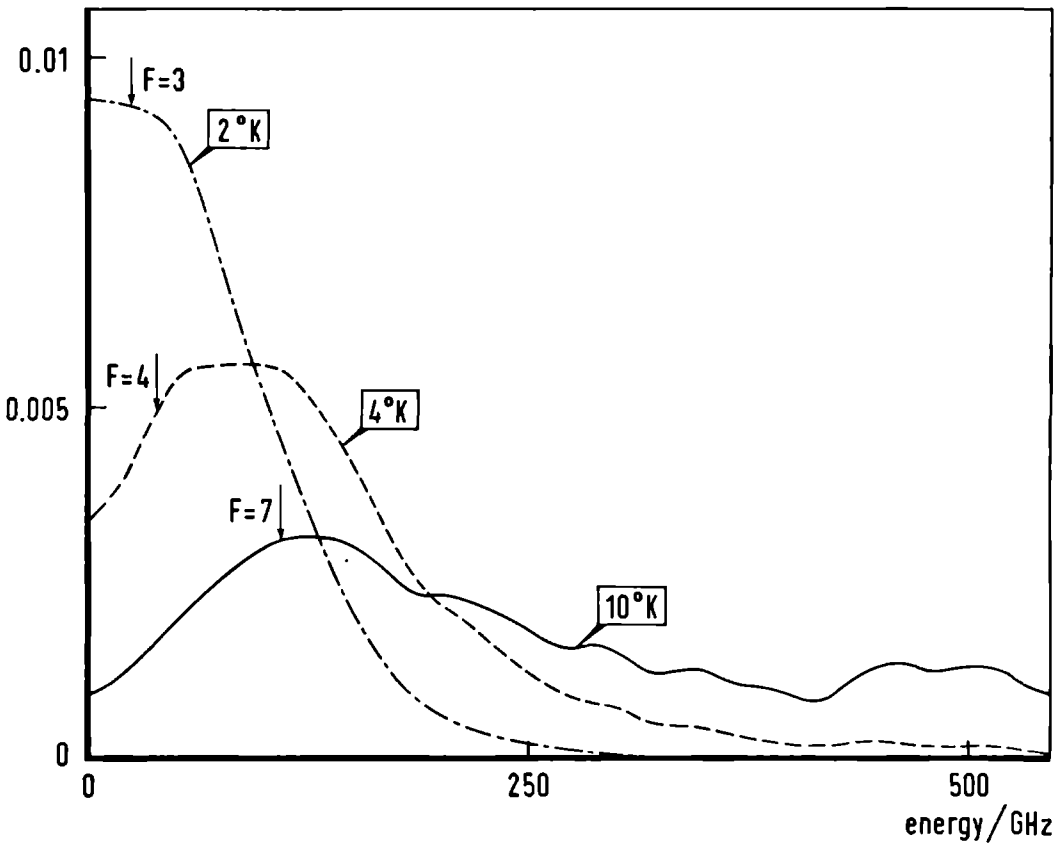

Fig. 2: Probability of finding the O_2Ar complex in a given energy region for several temperatures. The curves are smoothed and are normalised to unity. The state with the largest probability of occupation for each temperature is labeled by its F quantum number.

4. Zeeman splittings

We have calculated the splittings of our levels in a weak magnetic field using the perturbative Hamiltonian (10). Table 3 presents our results for the lowest states with $F \leq 3$. As the selection rule for pure Zeeman transitions is $\Delta M_F = \pm 1$, we predict the transition frequencies to be $g_e \mu_B B$ times the splitting (which is a dimensionless quantity).

In pure O_2 the Zeeman splitting decreases with increasing J [12] and analysis of our matrix elements suggests the splittings in the dimer decrease with increase F. To illustrate this,the result with $F = 15$ has been included in Table 3. However, two of the low-lying levels, $F = 1\,e$ and $F = 3\,e$, show splittings an order of magnitude smaller than the other low F states. Analysis of the eigenvectors of these states shows that they are dominated by $J = 0$ basis functions, which give zero Zeeman splitting. This means small Zeeman splitting can be observed not only from states with large F but also from states which are predominantly $J = 0$.

Table 3

First-order Zeeman splittings, eq. (10), of the low-lying states calculated using the potential of Pirani and Vecchiocattivi. The dissociation energy of the unperturbed state is given for comparison.

F	parity	energy/GHz	$\langle \hat{S}_z \rangle$
1	e	-2610.22	0.0374
1	o	-2511.16	0.2838
2	e	-2562.78	0.3620
2	o	-2602.36	0.03817
3	e	-2590.58	0.0393
3	o	-2551.41	0.2122
15	e	-2152.99	0.0220

5. Conclusions

In this work we have compared the O_2Ar fine structure spectra calculated using two empirical potentials [13,14]. The predicted spectra are in good agreement despite differences in the potentials, which are reflected in the energy levels. These spectra bear little resemblance to the fine structure spectrum of pure O_2; they are strongly perturbed by the anisotropy in the interaction potential. Measurements of the O_2Ar spectrum could thus provide valuable information about the anisotropy in the potential and could test whether higher (V_4) terms in the Legendre expansion of the potential are indeed insignificant. A computer programme (see [21]), such as the one used in this paper, which provides a fast and reliable method of generating spectra from a potential can easily be used in the fashion of LeRoy and Van Kranendonk [2] as a method of inverting experimental data to give information about the potential.

We have also calculated transition intensities, relative signal to noise ratios, Boltzmann populations of dimer states at several temperatures and weak field Zeeman splittings. All these should encourage the observation of both fine structure and Zeeman spectra of O_2Ar and experimental work on this is now in progress [22].

Acknowledgement

We thank Prof. J. Reuss for suggesting the problem, Geert Brocks for making available his programme for generating numerical basis sets and Prof. Ad van der Avoird for his careful reading of the manuscript.

References

[1] R.J. Le Roy and J. Carley, Advan. Chem. Phys., 42, (1980) 353; see also J. Chem. Soc. Faraday Disc., "Van der Waals molecules", 73 (1982).

[2] R.J. Le Roy and J. van Kranendonk, J. Chem. Phys., 61 (1974) 4750.

[3] A.M. Dunker and R.G. Gordon, J. Chem. Phys., 64 (1976) 354 and 68 (1978) 700.

[4] S.L. Holmgren, M. Waldman and W. Klemperer, J. Chem. Phys. 67 (1977) 4414 and 69 (1978) 1661.

[5] J. Tennyson and B.T. Sutcliffe, J. Chem. Phys., 15th October (1982) and submitted (1982),

[6] J. Tennyson and A. van der Avoird, J. Chem. Phys., Dec. 1st (1982).

[7] G.H.L.A. Brocks and J. Tennyson, J. Mol. Spectrosc., submitted (1982).

[8] J. Verberne and J. Reuss, Chem. Phys., 50 (1980) 137 and 54 (1981) 189.

[9] M. Waaijer, M. Jacobs and J. Reuss, Chem. Phys., 63 (1981) 257 and M. Waaijer and J. Reuss, Chem. Phys., 63 (1981) 263.

[10] M. Waaijer, M. Jacobs and J. Reuss, Chem. Phys., 63 (1981) 247.

[11] W.M. Welch and M. Mizushima, Phys. Rev. A, 5 (1972) 2692.

[12] A. Amirav, U. Even, J. Jortner and L. Kleinman, J. Chem. Phys., 73 (1980) 4217.

[13] V. Mingelgrin and R.G. Gordon, J. Chem. Phys., 70 (1979) 3828.

[14] F. Pirani and F. Vecchiocattivi, Chem. Phys., 59 (1981) 387.

[15] M. Mizushima, "The Theory of Rotating Diatomic Molecules", (Wiley, New York, 1975) Chapter 5.

[16] A. Messiah, "Quantum Mechanics", Vol. II, (North-Holland, Amsterdam, 1961) p. 1076-8.

[17] A.R. Edmonds, "Angular Momentum in Quantum Mechanics", 2nd Ed. (Princeton University, Princeton, 1960).

[18] I.C. Percival and M.J. Seaton, Proc. Camb. Phil. Soc., 53 (1957) 654.

[19] M. Tinkham and M.W.P. Strandberg, Phys. Rev. 97 (1955) 937 and 951.

[20] G. Henderson and G. Ewing, J. Chem. Phys., 59 (1973) 2280.

[21] J. Tennyson, submitted to Computer Phys. Comms. (1982).

[22] J. Mettes, D. Lainée and J. Reuss

Fine-structure spectrum of O_2-rare gas Van der Waals molecules

Ad van der Avoird

Institute of Theoretical Chemistry
University of Nijmegen
Toernooiveld, Nijmegen
The Netherlands

Abstract

A simple analytically solvable model is presented for the rotation-vibration-spin states in O_2-rare gas atom complexes, which predicts the form of the fine-structure spectrum. It is shown that this spectrum looks basically different from the pure O_2 spectrum, due to the partial quenching of the O_2 angular momentum by the anisotropic O_2-rare gas interaction potential. The model contains two properties of the O_2X complex as parameters: the ground state average of the anisotropic potential $\langle V_2(R)\rangle_0$ and the end-over-end rotational constant $\langle R^{-2}\rangle_0$, where R is the O_2-X distance. Adjusting these parameters yields quantitative agreement with the spectra that have recently been obtained from two different empirical potentials via accurate dynamical calculations. The model can be used for interpreting the experimental fine-structure spectrum of O_2Ar which is currently being measured.

PACS numbers: 33.10.Lb, 36.40.+d, 31.70.-f.

In a recent paper [1] Tennyson and Mettes report accurate dynamical calculations of the rotation-vibration-electron spin states in O_2Ar. From these calculations they obtain the fine-structure transition frequencies and intensities. Two features are especially noteworthy. First, their spectrum of O_2Ar looks very different from the pure O_2 spectrum. This is not only of practical interest in view of the measurements (where to find lines in the microwave or radiofrequency beam resonance experiments which are now carried out [2]?), but it is also interesting since the deviation from the pure O_2 spectrum is expected to be a measure of the anisotropy in the O_2-Ar interaction potential (if O_2Ar were bound by a purely isotropic interaction, its fine-structure spectrum would be identical to the O_2 spectrum). On the other hand, they found that two rather different empirical O_2-Ar potentials [3,4] yield strikingly similar fine-structure spectra (changing the anisotropy in one of the potentials [4] by a factor of 2 did affect the frequencies, however).

In view of these numerical results [1] and the interpretation of the measurements which are in progress [2], it is important to understand why the spectrum of O_2Ar differs from O_2, how the differences depend explicitly on the anisotropy of the potential and which transitions yield the most accurate information about the potential and other properties of the complex. In the present paper, it is shown how these questions can be answered by adopting a simple, but realistic, model for the rotation-vibration-electron spin states of O_2Ar (and other O_2X complexes, X = rare gas atom) which can be solved analytically.

The relevant hamiltonian can be written [1] as:

$$\hat{H} = \hat{H}_{rot\text{-}vib} + \hat{H}_{fine} \qquad (1)$$

where $\hat{H}_{rot\text{-}vib}$ is the usual rotation-vibration hamiltonian for an atom-rigid diatom complex:

$$\hat{H}_{rot\text{-}vib} = -\frac{\hbar^2}{2\mu R}\frac{\partial^2}{\partial R^2} R + B(R)\,\hat{\underline{L}}^2 + b\,\hat{\underline{N}}^2 + V(R,\theta). \qquad (2)$$

The vector $\underline{R} = (R,\beta,\alpha)$ connects the O_2 mass centre with the rare gas atom X, the vector $\underline{r} = (r_0,\delta,\gamma)$ describes the (fixed) O_2 bond length r_0 and orientation and the angular momenta $\hat{\underline{L}}$ and $\hat{\underline{N}}$ are associated with the polar angles (β,α) and (δ,γ), respectively. All these angles are defined relative to an arbitrary space-fixed (SF) coordinate frame. The constant μ denotes the reduced mass: $\mu = m_X m_{O_2}/(m_X+m_{O_2})$, $B(R)$ the end-over-end rotational constant of O_2X: $B(R) = (2\mu R^2)^{-1}$, and b the O_2 rotational constant: $b = (m_0 r_0^2)^{-1} = 43.1$ GHz [5]. The potential $V(R,\theta)$ is conveniently expressed in Legendre polynomials in $(\cos\theta)$, where θ is the angle between $\underline{r}$ and $\underline{R}$:

$$V(R,\theta) = \sum_{\lambda} V_\lambda(R)\, P_\lambda(\cos\theta) \qquad (3)$$

For a homonuclear diatomic such as O_2 only terms with even λ occur. In addition to the isotropic potential $V_0(R)$, both the empirical O_2Ar potentials [3,4] used in the dynamical calculations [1] include only the anisotropic $V_2(R)$ term.

The O_2 molecule is considered to stay in the electronic ground state $^3\Sigma_g^-$. Its electronic orbital momentum is zero and the dominant effective spin coupling term is given by [5,6]:

$$\hat{H}_{fine} = \frac{2}{3}\lambda_0(3\hat{S}_\zeta^2 - \hat{\underline{S}}^2) \qquad (4)$$

with λ_0 = 59.5 GHz, $\hat{\underline{S}}$ denoting the electron spin momentum and $\hat{S}_\zeta$ its projection on the O_2 axis $\underline{r}$. The $\mu_0 \hat{\underline{N}}.\hat{\underline{S}}$ term included in [1], and other terms, have been omitted here, since they are of minor importance.

Tennyson and Mettes [1] have calculated the rotation-vibration-electron spin states of O_2Ar by diagonalizing the matrix of the hamiltonian (1) over the following basis:

$$\chi_q(R)|((NS)JL)FM_F\rangle \qquad (5)$$

where $\chi_q(R)$ denote numerical radial basis functions [7,8]. The angular momentum functions are products of spherical harmonics $Y_{N,M_N}(\delta,\gamma)$ and electron spin functions Θ_{S,M_S} coupled via Clebsch-Gordan coefficients to get basis functions $|J,M_J\rangle$, which are then coupled to spherical harmonics $Y_{L,M_L}(\beta,\alpha)$, in order to obtain eigenfunctions of the total angular momentum operators $\hat{\underline{F}}^2$ and $\hat{F}_Z$, which represent the exact angular quantum numbers of the system. Only basis functions with odd N have to be included, since the O_2 nuclei have spin zero and the electronic ground state wave function is odd with respect to inversion (remember that the term symbol $^3\Sigma_g^-$ refers to a molecular frame lying along the O_2 axis) [5,6]. The electron spin basis is restricted to the ground state triplet (S = 1). Convergence of the eigenvalues to within 0.3 GHz was reached for $q \leq 4$ and $N \leq 7$.

So far, all the terms in the hamiltonian (2) and (4), as well as the basis (5), have been expressed relative to a space-fixed frame (SF). Actually, it is more convenient to use a body-fixed frame (BF) with the z-axis lying along the O_2-X axis $\underline{R}$. This can be achieved by a rotation over two Euler angles (α,β) which are the polar angles of $\underline{R}$ in the SF frame. The hamiltonian, after this rotation, can be written as:

$$\hat{H}_{rot-vib} = -\frac{\hbar^2}{2\mu R}\frac{\partial^2}{\partial R^2}R + B(R)(\hat{\underline{F}} - \hat{\underline{J}})^2 + b\,\hat{\underline{N}}^2 + V(R,\theta) \qquad (6)$$

and

$$\hat{H}_{fine} = \frac{2}{3}\lambda_0(3\hat{S}_\zeta^2 - \hat{\underline{S}}^2) \qquad (7)$$

where the operators $\hat{\underline{N}}$, $\hat{\underline{S}}$, $\hat{\underline{J}}$ and $\hat{\underline{F}}$ are now expressed in body-fixed components ($\hat{F}_z^{BF} = \hat{J}_z^{BF} = \hat{N}_z^{BF} + \hat{S}_z^{BF}$ since $\hat{L}_z^{BF} = 0$) and the second term in $H_{rot-vib}$ is most conveniently expanded as:

$$B(R)(\hat{\underline{F}} - \hat{\underline{J}})^2 = B(R)(\hat{\underline{F}} - \hat{\underline{N}} - \hat{\underline{S}})^2$$

$$= B(R)\ [\hat{\underline{F}}^2 + \hat{\underline{N}}^2 + \hat{\underline{S}}^2 - 2(\hat{N}_z + \hat{S}_z)^2 + 2\,\hat{N}_z\hat{S}_z$$

$$-(\hat{N}_+\hat{F}_+ + \hat{N}_-\hat{F}_- + \hat{S}_+\hat{F}_+ + \hat{S}_-\hat{F}_-) + (\hat{N}_+\hat{S}_- + \hat{N}_-\hat{S}_+)] \qquad (8)$$

This transformation of the hamiltonian is an extension of the spin-free case [7-10]. The rotation over two Euler angles (α,β) rather than three leads to an unusual form for the components of $\hat{\underline{F}}$ (cf. refs. [8-10]); also, they do not commute with $\hat{\underline{N}}$ and $\hat{\underline{S}}$. The step-up/down operators are defined as: $\hat{N}_\pm = \hat{N}_x \pm i\hat{N}_y$, $\hat{S}_\pm = \hat{S}_x \pm i\hat{S}_y$ and $\hat{F}_\pm = \hat{F}_x \mp i\hat{F}_y$.

The basis (5) transforms into:

$$\chi_q(R) \sum_K |((NS)JL)FK\rangle\, D^{(F)*}_{M_F,K}(\alpha,\beta,0) \qquad (9)$$

where the angular functions in the ket are now expressed in BF angles and the functions $D^{(F)}_{M_F,K}$ are rotation matrix elements [11]. Remembering that the polar angles of $\underline{R}$ are zero in the body-fixed frame and substituting the relation [11]: $Y_{L,M_L}(0,0) = \left(\frac{2L+1}{4\pi}\right)^{\frac{1}{2}} \delta_{M_L,0}$, so that $M_J = K$, one can replace (9) by an equivalent basis:

$$\chi_q(R)\,|(NS)JK\rangle\, D^{(F)*}_{M_F,K}(\alpha,\beta,0) \qquad (10)$$

In eqs. 9 ÷ 13 a normalisation factor is omitted.

The latter basis corresponds to the intermediate quantum numbers N, S, J and K, in addition to the exact quantum numbers F and M_F, while the basis (5) or (9) corresponds to N,S,J and L.The basis of eqs.(5) and (9) would be most appropriate when the anisotropy in the potential is very weak, as it is in H_2X complexes [7].

The basis (10) is still not the most efficient one for our problem, however, since the anisotropic ($\lambda \neq 0$) terms in the potential (3) will split the energy levels of different M_N states. Basis functions with N = 1, for instance, will be split by the $\lambda = 2$ term in the potential into levels $\langle V_0(R)\rangle - \frac{1}{5}\langle V_2(R)\rangle$ for $M_N = \pm 1$ and levels $\langle V_0(R)\rangle + \frac{2}{5}\langle V_2(R)\rangle$ for $M_N = 0$. So, if $\langle V_2(R)\rangle$ is positive, which corresponds to a T-shaped O_2X complex, and sufficiently large, then the functions with $M_N = 0$ will be raised in energy to such an extent that they will hardly mix into the lower states of the complex (see next section). This destroys J as a good intermediate quantum number. A basis which reflects this splitting is the uncoupled product basis:

$$\chi_q(R)\; Y_{N,M_N}(\theta,\phi)\; \Theta_{S,M_S}\; D^{(F)*}_{M_F,K}(\alpha,\beta,0) \qquad (11)$$

where (θ,ϕ) are the polar angles of $\underline{r}$ in the BF system and also the components (M_S) of the spin functions Θ_{S,M_S} are expressed relative to this system. The elements of this basis are eigenfunctions of the operators $\hat{\underline{N}}^2$, $\hat{N}_z$, $\hat{\underline{S}}^2$, $\hat{S}_z$, $\hat{F}^{BF}_z$, $\hat{\underline{F}}^2$ and $\underline{F}^{SF}_z$ with eigenvalues N(N+1), M_N, S(S+1), M_S, K, F(F+1) and M_F, respectively [8-10], and $K = M_N + M_S$.

Finally, it is useful to consider the behaviour of the bases under inversion. The SF basis (5),including the electronic wave function,has parity $(-1)^{N+S+L+1}$. The BF basis (11) for $(M_N,M_S) \neq (0,0)$ has to be adapted to inversion:

$$\frac{1}{\sqrt{2}}\chi_q(R)\left[Y_{N,M_N}\Theta_{S,M_S}D^{(F)*}_{M_F,K} + (-1)^p Y_{N,-M_N}\Theta_{S,-M_S}D^{(F)*}_{M_F,-K}\right] \qquad (12)$$

Then, again including the odd parity electronic $^3\Sigma_g^-$ wave function, the total parity becomes $(-1)^{p+F+1}$.

a. First order model

Starting from the product basis (11) in a BF frame, one can make a number of simplifying assumptions regarding the lower rotation-vibration-spin states in O_2X complexes. It has been observed already that the O_2 molecule can be considered to remain in its electronic ground state, which corresponds to a triplet spin function: $S = 1$, $M_S = -1,0,1$. Actually, the admixture of electronically excited states via spin-orbit coupling is already taken into account [5,6] in the effective spin hamiltonian (7). Basis functions with $N = 1$ are lowest in energy, while basis functions with the next higher O_2 rotational quantum number, $N = 3$, are raised by the term $b\hat{\underline{N}}^2$ in the hamiltonian (6) to an energy that is $10\,b = 431$ GHz higher. The rotation barrier Δ in O_2Ar from the T-shaped equilibrium structure to the linear structure is about 30 cm^{-1} [12], which corresponds to an anisotropic potential $V_2(R) = \frac{2}{3}\Delta \simeq 20\ cm^{-1} \simeq 600$ GHz in the range of the Van der Waals minimum $R \simeq R_e$. It is mentioned already in the previous section that this anisotropy raises the energy of the $N = 1$, $M_N = 0$ states relative to the $N = 1$, $M_N = \pm 1$ states by $\frac{3}{5} V_2(R) \simeq 360$ GHz. Finally, one has to consider the radial (stretching) motion of the O_2-X complex. A reasonable estimate for the fundamental vibrational excitation energy in O_2Ar is 30 $cm^{-1} \simeq 900$ GHz (cf. the Ar_2 value of 28 cm^{-1} [13]).

Given all these energy differences, one might assert that the lower rotation-vibration-spin states of O_2Ar (and other O_2X complexes) within, say, 200 GHz from the ground state are mainly composed of basis functions:

$$\phi_0(R)\ Y_{N,M_N}(\theta,\phi)\ \Theta_{S,M_S}\ D^{(F)*}_{M_F,K}(\alpha,\beta,0) \qquad (13)$$

with:

$N = 1$, $M_N = \pm 1$, $S = 1$ and $M_S = 0, \pm 1$,

where $\phi_0(R)$ is the stretch ground state wave function ($v_s = 0$), which could be

obtained, numerically or as a linear combination of functions $\chi_q(R)$ (cf. the basis (11)), from a radial (one-dimensional) equation with the effective potential $V_0(R) - \frac{1}{5}V_2(R)$. This effective potential corresponds exactly with the complete anisotropic potential [3,4] if one can indeed restrict the ground state basis to $N = 1$, $M_N = \pm 1$.

The first order model proposed consists of diagonalizing the full rotation-vibration-spin hamiltonian, eqs. (6) and (7), in a zero order BF basis (13) which is degenerate with respect to the "unperturbed" hamiltonian:

$$\hat{H}_0 = -\frac{\hbar^2}{2\mu R}\frac{\partial^2}{\partial R^2}R + b\hat{\underline{N}}^2 + \sum_{\lambda=0,2} V_\lambda(R)P_\lambda(\cos\theta) \qquad (14)$$

with eigenvalue:

$$E_0 = \langle -\frac{\hbar^2}{2\mu R}\frac{\partial^2}{\partial R^2}R\rangle_0 + 2b + \langle V_0(R)\rangle_0 - \frac{1}{5}\langle V_2(R)\rangle_0 = \epsilon_{v_s=0} + 2b \qquad (15)$$

where $\langle\ \rangle_0$ denotes the radial ground state expectation value over $\phi_0(R)$.

The perturbation matrix elements are, using (8), with $B = \langle B(R)\rangle_0 = \langle R^{-2}\rangle_0/2\mu$:

$$\langle N\ M_N'\ S\ M_S'\ K'\ F\ M_F|B(R)(\hat{\underline{F}} - \hat{\underline{J}})^2|N\ M_N\ S\ M_S\ K\ F\ M_F\rangle =$$

diagonal: $$B\,F(F+1) + B\,N(N+1) + B\,S(S+1) - 2B\,K^2 + 2B\,M_N M_S \qquad (16a)$$

off-diagonal: $$B[F(F+1) - K(K\pm 1)]^{\frac{1}{2}}\,[S(S+1) - M_S(M_S \pm 1)]^{\frac{1}{2}} \qquad (16b)$$
$(M_N' = M_N\ \ )$
$(M_S' = M_S \pm 1)$
$(K' = K \pm 1\ )$

$$\langle N\ M_N'\ S\ M_S'\ K'\ F\ M_F|\tfrac{2}{3}\lambda_0(3\hat{S}_\zeta^2 - \hat{\underline{S}}^2)|N\ M_N\ S\ M_S\ K\ F\ M_F\rangle =$$

diagonal: $$\frac{2}{3}\lambda_0(-1)^{N+S-K}\begin{pmatrix} N & 2 & N \\ -M_N & 0 & M_N\end{pmatrix}\begin{pmatrix} S & 2 & S \\ -M_S & 0 & M_S\end{pmatrix}\langle N\|C_2\|N\rangle\langle S\|N_2\|S\rangle \qquad (17a)$$

off-diagonal:
$(-M'_N = M_N = \pm 1)$
$(-M'_S = M_S = \mp 1)$
$(K' = K = 0)$

$$\frac{2}{3}\lambda_0(-1)^{N+S}\begin{pmatrix} N & 2 & N \\ M_N & \mp 2 & M_N \end{pmatrix}\begin{pmatrix} S & 2 & S \\ M_S & \pm 2 & M_S \end{pmatrix}\langle N\|C_2\|N\rangle\langle S\|U_2\|S\rangle \qquad (17b)$$

The latter matrix elements can be derived by expanding the BF spin hamiltonian:

$$3\hat{S}_\zeta^2 - \underline{\hat{S}}^2 = \sum_q (-1)^q C_{2,q}(\theta,\phi)\, U_{2,-q}(\underline{\hat{S}}) \qquad (18)$$

in terms of second rank tensors [5] and using the Wigner-Eckart theorem [11]. The reduced matrix elements are:

$$\langle N'\|C_2\|N\rangle = (-1)^{N'}\,[(2N'+1)(2N+1)]^{\frac{1}{2}}\begin{pmatrix} N' & 2 & N \\ 0 & 0 & 0 \end{pmatrix} \qquad (19a)$$

and

$$\langle S\|U_2\|S\rangle = [(S(S+1)(2S-1)(2S+1)(2S+3)]^{\frac{1}{2}} \qquad (19b)$$

The larger round brackets denote 3-j symbols [11].

Thus, the (first order) secular matrix for the 6-dimensional zeroth order space (13) can be calculated. All the terms are diagonal in K ($K' = K$) except for the "Coriolis" terms (16b). In first instance, I shall neglect these terms, making K a good quantum number and the secular matrix diagonal, except for the element (17b) between the two $K = 0$ basis functions. These basis functions are connected by inversion symmetry and by adapting the basis to this symmetry according to eq. (12), using the quantum numbers $|K|$ and p, the secular matrix becomes completely diagonal. The first order results, summarized in Table 1, are extremely simple. Still, they are very interesting as they show that the eigenvalue spectrum of O_2X complexes in the low energy region consists of 4 rotational ladders: $\varepsilon_i + B\,F(F+1)$, $i = 1,2,3,4$ with $B = \langle B(R)\rangle_0$ being the O_2X end-over-end

Table 1. Results of the first order model

i	eigenstates $\|N,M_N;S,M_S;K,F\rangle$ (multiplicity $2F+1$)	$\|K\|$	$(-1)^p$	total parity	first order energy, relative to ground level
1	$\frac{1}{\sqrt{2}}(\|1,1;1,-1;0,F\rangle + \|1,-1;1,1;0,F\rangle)$	0	+	$-(-1)^F$	$BF(F+1)$
2	$\frac{1}{\sqrt{2}}(\|1,1;1,1;2,E\rangle \pm \|1,-1;1,-1;-2,E\rangle)$	2	±	$\mp(-1)^F$	$\frac{4}{5}\lambda_0 - 4B + BF(F+1)$
3	$\frac{1}{\sqrt{2}}(\|1,1;1,0;1,F\rangle \pm \|1,-1;1,0;-1,F\rangle)$	1	±	$\mp(-1)^F$	$\frac{6}{5}\lambda_0 + BF(F+1)$
4	$\frac{1}{\sqrt{2}}(\|1,1;1,-1;0,F\rangle - \|1,-1;1,1;0,F\rangle)$	0	-	$(-1)^F$	$\frac{8}{5}\lambda_0 + BF(F+1)$

rotational constant. Each ladder (i) corresponds with a definite ($|K|$,p) quantum number and the ladders start at different rungs, since the quantum numbers F labeling the "rotational" levels, must satisfy the relation $F \geq |K|$. The lowest (i = 1) and the highest (i = 4) ladder, both with K = 0, have levels of definite parity, alternating with F, while the rungs of the middle two ladders (i = 2,3), $|K| = 2$ and $|K| = 1$, are doublets of both + and - parity.

Actually, these doublets will be split by the off-diagonal Coriolis terms (16b) which I have neglected so far.For the $|K| = 2$ ladder this splitting will be very small as there is only direct coupling with the $|K| = 1$ states, which yields equal shifts of the + and - levels. The $|K| = 1$ states mix with K = 0 states (of the same F and parity) and since the + and - states of the latter (for a given F) belong to the two different K = 0 ladders, one obtains a splitting of order $B^2F(F+1)S(S+1)[(\varepsilon_3 - \varepsilon_1)^{-1} - (\varepsilon_3 - \varepsilon_4)^{-1}]$ (the sign of this splitting alternates with F).

This model predicts the complete structure of the eigenvalue spectrum of O_2X complexes in the range between 0 and 200 GHz. The fine-structure transition frequencies can be obtained from the differences between these eigenvalues and the (dipole) selection rules [1]: $\Delta F = 0$ or ± 1, $\pm \nleftrightarrow \pm$ for magnetic dipoles, $\pm \nleftrightarrow \mp$ for electric dipoles. Looking at the results of Tennyson and Mettes [1], one can observe that, indeed, accurate numerical calculations for O_2Ar yield a spectrum of this shape for both empirical potentials [3,4]. This is clearly shown in fig. 1. Table 1 of reference [1] contains the frequencies of transitions between the different ladders as well as transitions within the same ladders. From the splittings within the ladders one can deduce that $B = \langle B(R) \rangle_0$ equals 1.97 GHz for the PV potential [4] and 2.04 GHz for the MG potential [3], which corresponds with an average O_2-Ar distance of $\langle R^{-2} \rangle_0^{-\frac{1}{2}} = 3.78$ Å and 3.71 Å, respectively. The splittings between the ladders are found to be ($\varepsilon_1 = 0$): $\varepsilon_2 = 39.6$ GHz, $\varepsilon_3 = 99.6$ GHz and $\varepsilon_4 = 111.8$ GHz for the PV potential and $\varepsilon_2 = 39.4$ GHz, $\varepsilon_3 = 101.3$ GHz and $\varepsilon_4 = 112.3$ GHz for the MG potential, whereas the first order model predicts:

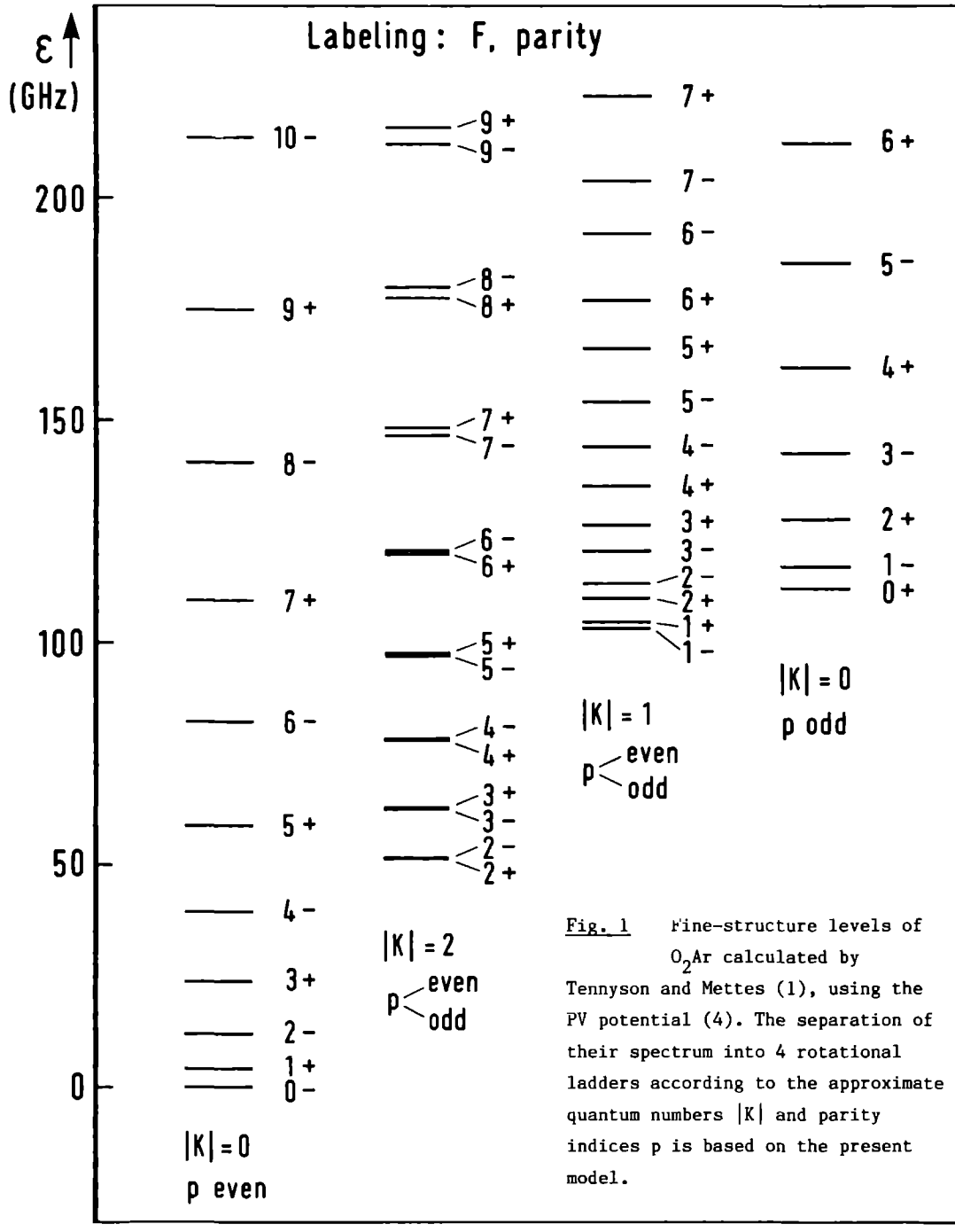

Fig. 1 Fine-structure levels of O_2Ar calculated by Tennyson and Mettes (1), using the PV potential (4). The separation of their spectrum into 4 rotational ladders according to the approximate quantum numbers |K| and parity indices p is based on the present model.

ε_2 = 39.7 GHz, ε_3 = 71.4 GH_z and ε_4 = 95.2 GHz, independently of the potential (provided that $\langle V_2(R)\rangle_0$ is sufficiently large to make (13) a good zeroth order basis). Although the agreement is not unsatisfactory, considering the crudeness of the model, it can still be improved significantly via simple 2^{nd} order corrections.

b. Second order model

In order to obtain not just qualitative, but also quantitative, agreement with the accurate calculations by Tennyson and Mettes [1], for the splittings between the 4 ladders, the first order model should be extended. Moreover, this will tell us how sensitive these splittings are to the anisotropy of the potential.

The zeroth order eigenstates and the first order eigenvalues (Table 1) can be improved by the admixture of higher unperturbed states. The dominant excited states are probably the states with N = 1, M_N = 0, which lie above the ground state by $\frac{3}{5}\langle V_2(R)\rangle_0 \simeq 360$ GHz (see preceding section), and the N = 3 states which are higher than the N = 1 states by 10 B = 431 GHz. The next higher, N = 5, states correspond with an excitation energy 28 B = 1207 GHz, which is considerably higher again. Moreover, the N = 5 states are not directly coupled to the ground (N = 1) state.

Both the N = 1, M_N = 0 and the N = 3, M_N = 0,±1,±2,±3 excited states (M_S = 0, ±1) are coupled to the ground state by the spin terms $\hat{H}_{fine}(7)$, while the N = 3, M_N = ±1 states are coupled by the anisotropic potential $V_2(R)\ P_2(\cos\theta)$ as well. Using first order perturbation theory [6] for the wave functions and second order expressions for the energy levels, the corrections can still be done analytically, see Table 2. The coupling matrix elements are:

$$\langle N'\ M_N'\ S\ M_S'\ F\ M_F | V_2(R)\ P_2(\cos\theta) | N\ M_N\ S\ M_S\ F\ M_F\rangle =$$

$$\langle V_2(R)\rangle_0 \, \delta_{M'_N,M_N} \, \delta_{M'_S,M_S} (-1)^{N'-M'_N} \begin{pmatrix} N' & 2 & N \\ -M_N & 0 & M_N \end{pmatrix} \langle N' \| C_2 \| N \rangle \qquad (20)$$

and:

$$\langle N' \; M'_N \; S \; M'_S \; F \; M_F | \hat{H}_{fine} | N \; M_N \; S \; M_S \; F \; M_F \rangle =$$

$$(-1)^{N'+S-M_N-M'_S} \, \delta_{K',K} \begin{pmatrix} N' & 2 & N \\ -M'_N & M'_N-M_N & M_N \end{pmatrix} \begin{pmatrix} S & 2 & S \\ -M'_S & M'_S-M_S & M_S \end{pmatrix} \langle N' \| C_2 \| N \rangle \langle S \| U_2 \| S \rangle \qquad (21)$$

with the reduced matrix elements given by (19).

The same correction procedure can be used for pure O_2. The first order model, in this case (Hund's coupling case b [5,6]), corresponds to taking a basis composed of spherical harmonics $Y_{N,M_N}(\theta,\phi)$ with N = 1 and spin functions Θ_{S,M_S} with S = 1, coupled to $|J \; M_J\rangle$ with J = 0,1 and 2 and calculating the expectation values of $\hat{H}_{fine}$ (7). The second order energy corrects for the admixture (also via $\hat{H}_{fine}$) of N = 3 functions, again coupled with S = 1. This affects only the J = 2 level; the correction is usually done by solving a two-dimensional secular problem [5,6]. From the results given in Table 3, it is evident that second order perturbation theory gives quite accurate results too.

For O_2X the results are shown in Table 4. Substituting reasonable values for the anisotropy parameter $V_2 = \langle V_2(R)\rangle_0$ in O_2Ar into the expressions of Table 2 yields quantitative agreement between the second order model splittings and the accurate numerical spectra calculated [1] from the empirical potentials [3,4].

Table 2. Second order corrections: $\varepsilon_i^{(2)} = \sum_{n_i}{}' \dfrac{|\langle 0_i|\bar{H}|n_i\rangle|^2}{\langle 0_i|\bar{H}|0_i\rangle - \langle n_i|\bar{H}|n_i\rangle}$

Ground state $\|0_i\rangle$	i	Excited states $\|n_i\rangle$, labeled by $\|N,M_N;S,M_S\rangle$			
$\frac{1}{\sqrt{2}}[\|1,1;1,-1\rangle + \|1,-1;1,1\rangle]$	1	$\|1,0;1,0\rangle$	$\|3,0;1,0\rangle$	$\frac{1}{\sqrt{2}}[\|3,1;1,-1\rangle + \|3,-1;1,1\rangle]$	
$\varepsilon_1^{(1)} = 0$	$\varepsilon_1^{(2)}$:	$\dfrac{-\frac{8}{25}\lambda_0^2}{\frac{3}{5}V_2 + \frac{2}{5}\lambda_0}$	$\dfrac{-\frac{24}{175}\lambda_0^2}{10B + \frac{7}{15}V_2 + \frac{26}{45}\lambda_0}$	$\dfrac{-\frac{2}{175}(3V_2 + 4\lambda_0)^2}{10B + \frac{2}{5}V_2 + \frac{8}{15}\lambda_0}$	
$\frac{1}{\sqrt{2}}[\|1,1;1,1\rangle \pm \|1,-1;1,-1\rangle]$	2	$\frac{1}{\sqrt{2}}[\|3,3;1,-1\rangle \pm \|3,-3;1,1\rangle]$	$\frac{1}{\sqrt{2}}[\|3,2;1,0\rangle \pm \|3,-2;1,0\rangle]$	$\frac{1}{\sqrt{2}}[\|3,1;1,1\rangle \pm \|3,-1;1,-1\rangle]$	
$\varepsilon_2^{(1)} = \frac{4}{5}\lambda_0 - 4b$	$\varepsilon_2^{(2)}$:	$\dfrac{-\frac{24}{35}\lambda_0^2}{10B - \frac{2}{15}V_2 - \frac{4}{45}\lambda_0}$	$\dfrac{-\frac{8}{35}\lambda_0^2}{10B + \frac{1}{5}V_2 + \frac{2}{15}\lambda_0}$	$\dfrac{-\frac{2}{175}(3V_2 + 2\lambda_0)^2}{10B + \frac{2}{5}V_2 + \frac{4}{15}\lambda_0}$	
$\frac{1}{\sqrt{2}}[\|1,1;1,0\rangle \pm \|1,-1;1,0\rangle]$	3	$\frac{1}{\sqrt{2}}[\|1,0;1,1\rangle \pm \|1,0;1,-1\rangle]$	$\frac{1}{\sqrt{2}}[\|3,2;1,-1\rangle \pm \|3,-2;1,1\rangle]$	$\frac{1}{\sqrt{2}}[\|3,1;1,0\rangle \pm \|3,-1;1,0\rangle]$	$\frac{1}{\sqrt{2}}[\|3,0;1,1\rangle \pm \|3,0,1,-1\rangle]$
$\varepsilon_3^{(1)} = \frac{6}{5}\lambda_0$	$\varepsilon_3^{(2)}$:	$\dfrac{-\frac{4}{25}\lambda_0^2}{\frac{3}{5}V_2}$	$\dfrac{-\frac{8}{35}\lambda_0^2}{10B + \frac{1}{5}V_2 - \frac{4}{15}\lambda_0}$	$\dfrac{-\frac{2}{175}(3V_2 - 4\lambda_0)^2}{10B + \frac{2}{5}V_2 - \frac{8}{15}\lambda_0}$	$\dfrac{-\frac{12}{175}\lambda_0^2}{10B + \frac{7}{15}V_2 - \frac{4}{45}\lambda_0}$
$\frac{1}{\sqrt{2}}[\|1,1;1,-1\rangle - \|1,-1;1,1\rangle]$	4			$\frac{1}{\sqrt{2}}[\|3,1;1,-1\rangle - \|3,-1;1,1\rangle]$	
$\varepsilon_4^{(1)} = \frac{8}{5}\lambda_0$	$\varepsilon_4^{(2)}$:			$\dfrac{-\frac{18}{175}V_2^2}{10B + \frac{2}{5}V_2}$	

Table 3. Second order model results for O_2

	$\varepsilon^{(1)}$	$\varepsilon^{(2)}$	$\varepsilon^{(1)}+\varepsilon^{(2)}$	exact splittings from $\hat{H}_{fine}$	experimental [5]
$\varepsilon(J=2) - \varepsilon(J=0)$:	$\frac{6}{5}\lambda_0 = 71.4$ GHz	$\frac{-\frac{24}{25}\lambda_0^2}{10b} = -7.9$ GHz	63.5 GHz	63.2 GHz	62.5 GHz
$\varepsilon(J=1) - \varepsilon(J=0)$:	$2\lambda_0 = 119.0$ GHz	0	119.0 GHz	119.0 GHz	118.8 GHz

Table 4. Second order model results for O_2Ar

(splittings between the 4 ladders in GHz)

	$\varepsilon^{(1)}$	$\varepsilon^{(1)} + \varepsilon^{(2)}$ for:				accurate dynamical calculations [1]	
		V_2 = 450 ,	600 ,	750 ,	900 GHz	with PV potential [4]	with MG potential [3]
$\varepsilon_2-\varepsilon_1$ *)	39.7/39.4	41.7/41.4	41.2/40.9	40.8/40.5	40.5/40.2	39.6	39.4
$\varepsilon_3-\varepsilon_1$	71.4	92.3	95.5	98.0	99.9	99.6	101.3
$\varepsilon_4-\varepsilon_1$	95.2	110.5	111.2	111.8	112.3	111.8	112.3

*) calculated with B = 1.97 and 2.04 GHz for the PV and MG potentials, respectively.

From a very simple, first order, model (see Table 1) I have derived the general structure of the fine-structure spectrum in O_2Ar (see fig. 1). Although the O_2-Ar interaction is a weak Van der Waals bond, this spectrum is fundamentally different from the pure O_2 spectrum (cf. Table 3). The differences are shown to be caused by the partial quenching of the free O_2 rotations by the anisotropic O_2Ar interaction potential. This anisotropy makes the projection $|K| = |M_N + M_S|$ of the O_2 angular momentum $\underline{J} = \underline{N} + \underline{S}$ on the O_2Ar-axis a (nearly) good quantum number, rather than the total diatom angular momentum J. The fine-structure spectrum thus obtained is typical for a T-shaped O_2X (X = rare gas atom) complex. For the linear case, if it exists, one can easily work out a similar model.

Adding (still analytical) second order corrections (Table 2) to the energy level splittings yields quantitative agreement (see Table 4) between the model spectrum and the data from accurate dynamical calculations [1], which have started from two different empirical anisotropic O_2Ar potentials [3,4]. The model shows explicitly how the transition frequencies depend on the strength of the anisotropic potential $V_2 = \langle V_2(R) \rangle_0$ and the value of the end-over-end rotational constant $B = \langle B(R) \rangle_0 = \langle R^{-2} \rangle_0 / 2\mu$. This will be useful for interpreting the experimental O_2Ar fine-structure spectrum which is currently being experimentally studied [2]. If one wishes to exploit the full precision of the experimental beam resonance data, one should still perform accurate numerical calculations, such as those by Tennyson and Mettes [1]. However, it will probably be necessary also to improve the existing empirical potentials, for instance by the inclusion of higher anisotropic V_4 terms. The secular problem to be solved is simplified and convergence can be accelerated by using a body-fixed basis of the type (13), including higher rotational $N = 3,5,\ldots$ and stretch vibrational ($\phi_{v_s}(R)$, with $v_s = 1,2,\ldots$) components (rather than the space-fixed basis (5) with stretch functions $\chi_q(R)$ derived from the isotropic potential [1]).

Acknowledgement

I would like to thank Jacques Mettes and Jonathan Tennyson for giving me their detailed results and for useful discussions. I have also had stimulating discussions on this subject with Geert Brocks and professor Jörg Reuss.

References

1. J. Tennyson and J. Mettes, Chem. Phys., accepted.
2. J. Mettes, D. Lainé and J. Reuss, private communication.
3. V. Mingelgrin and R.G. Gordon, J. Chem. Phys. 70 (1979) 3828.
4. F. Pirani and F. Vecchiocattivi, Chem. Phys. 59 (1981) 387.
5. M. Mizushimá, The Theory of Rotating Diatomic Molecules, Wiley, New York (1975).
6. L.D. Landau and E.M. Lifshitz, Course of Theoretical Physics, Vol. 3, Quantum Mechanics, Pergamon, Oxford (1958).
7. R.J. Le Roy and J.S. Carley, Advan. Chem. Phys., 42 (1980) 353.
8. G. Brocks and J. Tennyson, J. Mol. Spectrosc., submitted (1982).
9. G. Brocks, Internal Report, Institute of Theoretical Chemistry, Nijmegen (1982).
10. J. Tennyson and A. van der Avoird, J. Chem. Phys. 77 (1982) 5664.
11. D.M. Brink and G.R. Satchler, Angular Momentum, Clarendon, Oxford (1968).
12. G. Henderson and G.E. Ewing, J. Chem. Phys. 59 (1973) 2280.
13. H.P. Godfried and I.F. Silvera, Phys. Rev. Letters 48 (1982) 1337.

METHOD TO DETERMINE THE ROTATIONAL TEMPERATURE IN A MOLECULAR BEAM, DEMONSTRATED ON O_2

J. Mettes[+], B. Heijmen[+], D.C. Lainé[++] and J. Reuss[+]

[+] Fysisch Laboratorium, Katholieke Universiteit
Toernooiveld, 6525 ED Nijmegen, The Netherlands

[++] Physics Department, University of Keele,
Keele, Staffordshire ST5 5BG, U.K.

ABSTRACT

A novel method of general applicability is presented for the experimental determination of rotational temperature in a molecular beam, which is based on measurements of beam intensity versus stagnation pressure for both total flow and a single transition. Illustrative results are presented for r.f. and microwave transitions of $^{16}O^{16}O$

INTRODUCTION

Measurement of rotational molecular beam temperature is often difficult because when a comparison of the relative intensities of either two microwave or two radio-frequency lines is to be used for this purpose, then knowledge of the relative transition strengths is needed if a weak unsaturated absorption is employed. These difficulties are essentially circumvented by the use of a pair of saturated transitions (if saturation is possible) but even then difficulties arise in accurate temperature measurements due to the problem that slightly different trajectories in the molecular beam machine (electric beam resonance - EBR, and magnetic beam resonance - MBR) are taken by molecules in the two associated quantum states, for which a correction should be made [1]. An experimental method is reported in this paper that bypasses the difficulties of a comparison of relative intensities of two or more spectral lines. Although the temperature measurement method discussed here is based on a single spectral line, it is neither necessary to know its matrix elements, nor to saturate the transition in an experimental measurement. The experimental procedure necessitates measurements of the relative beam intensities for both the total flow of molecules and those molecules which undergo a resonant transition, as a function of the stagnation pressure. This routine may be applied to radio-frequency, microwave and, in principle, also laser transitions.

Other methods for temperature measurements are based on e.g. energy balance [2], IR-fluorescence [3], Raman-effect [4,5], laser induced fluorescence [6,7], electron fluorescence [8], infrared absorption [9], molecular beam electric and magnetic resonance spectroscopy [1,10] and masers [11].

As an example, results for the oxygen molecule are presented using both r.f. and 60 GHz transitions of $^{16}O^{16}O$. (The microwave transition is facilitated by the use of a widely tunable semi-open resonator whose properties are described in detail in the appendix). Previous work performed with the present MBR-machine (state selection for collision measurements, H_2 dimer spectroscopy) can be found in [10,12,13, 14]; Zeeman spectra of the O_2-Ar complex are being measured at this moment.

The detected signal I of beam intensity probes a certain energy level, with quantum numbers (N,J) in the case of O_2. The intensity I may be factorized into two functions; the first is proportional to the total flow of molecules F, the second is the relative population of the energy level (N,J). Thus

$$I(N,J,P_0) \propto F(P_0)\ \exp(-E(N,J)/kT(P_0))/Z \qquad (1)$$

where Z is the partition function, which for the case of O_2 is given by

$$Z = \sum_{N'=1,3,\ldots} \sum_{J'=N'-1,N',N'+1} (2J'+1)\exp(-E(N',J')/kT(P_0)) \qquad (2)$$

where T is the relevant temperature and P_0 the stagnation pressure.

The beam intensity I is measured as a function of stagnation pressure using lock-in detection and chopped transition-exciting radiation. The total molecular beam flow F (or a quantity proportional to F) is measured as a function of P_0 using a mechanical chopper and lock-in detection. From the ratio of the experimental functions $I(P_0)$ and $F(P_0)$ a function is obtained which henceforth is referred to as $X = I(P_0)/F(P_0)$ and which is proportional to the population of the level (N,J). Examples of such functions X can be seen in figure 1, each of which displays a single maximum.

For a thermal distribution the fractional population n of the (N,J) level as function of T can be caculated from

$$n(N,J,T) = \exp(-E(N,J)/kT)/Z \qquad (3)$$

Examples are shown in figures 2 and 3. Comparison of X with n yields T as a function of P_0. The maximum of the experimental curve $X(P_0)$ is found at the stagnation pressure $P_0 = P_0'$; the maximum of the theoretical curve n(T) is found at the temperature $T = T'$; thus for the stagnation pressure P_0' the rotational temperature is T'. For half maximum values the procedure is similar. This method assumes a thermal distribution

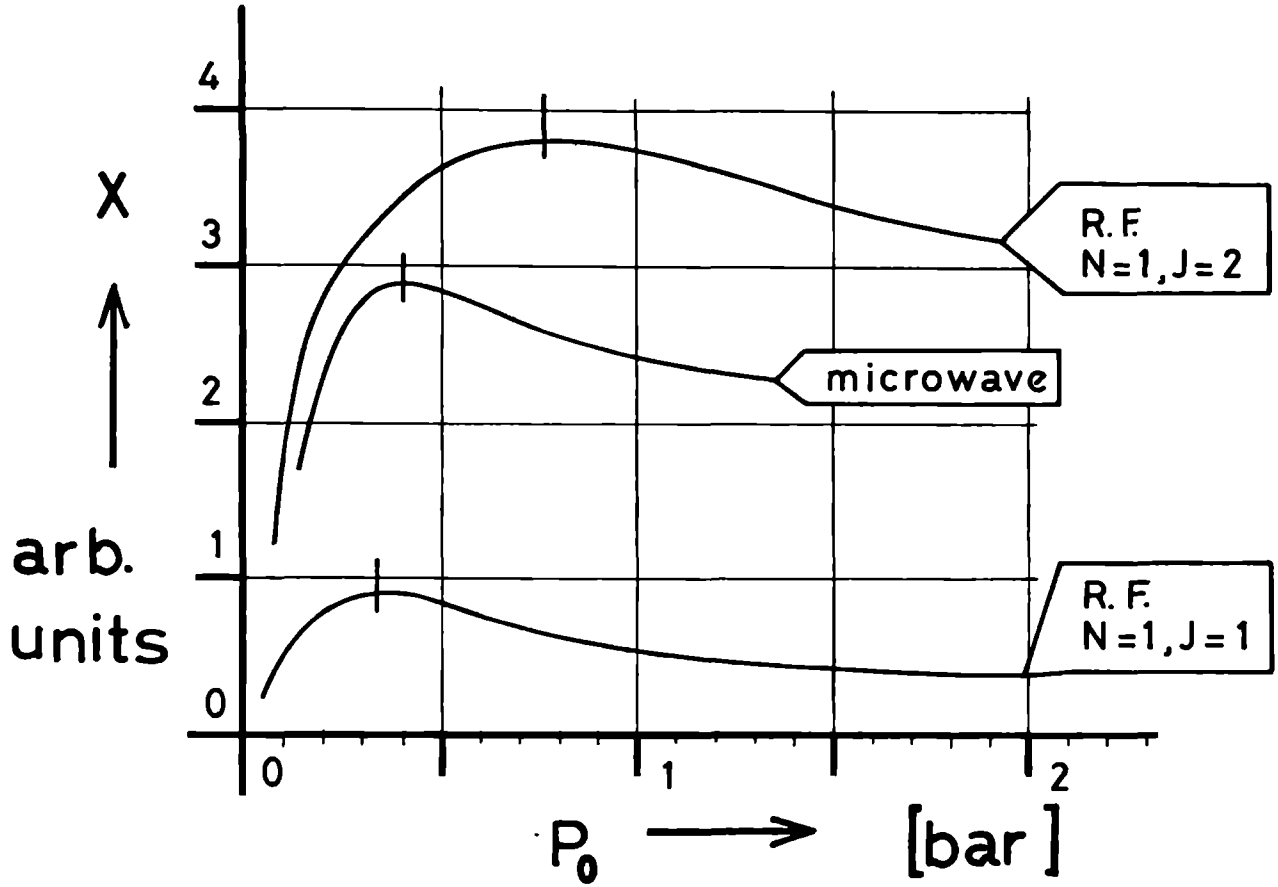

figure 1. Experimental plot for the two r.f. and single microwave transitions. The microwave result shows its maximum at a P_0 value in between the P_0 values of the maxima of the r.f. results (probing final and initial levels of the microwave transition).

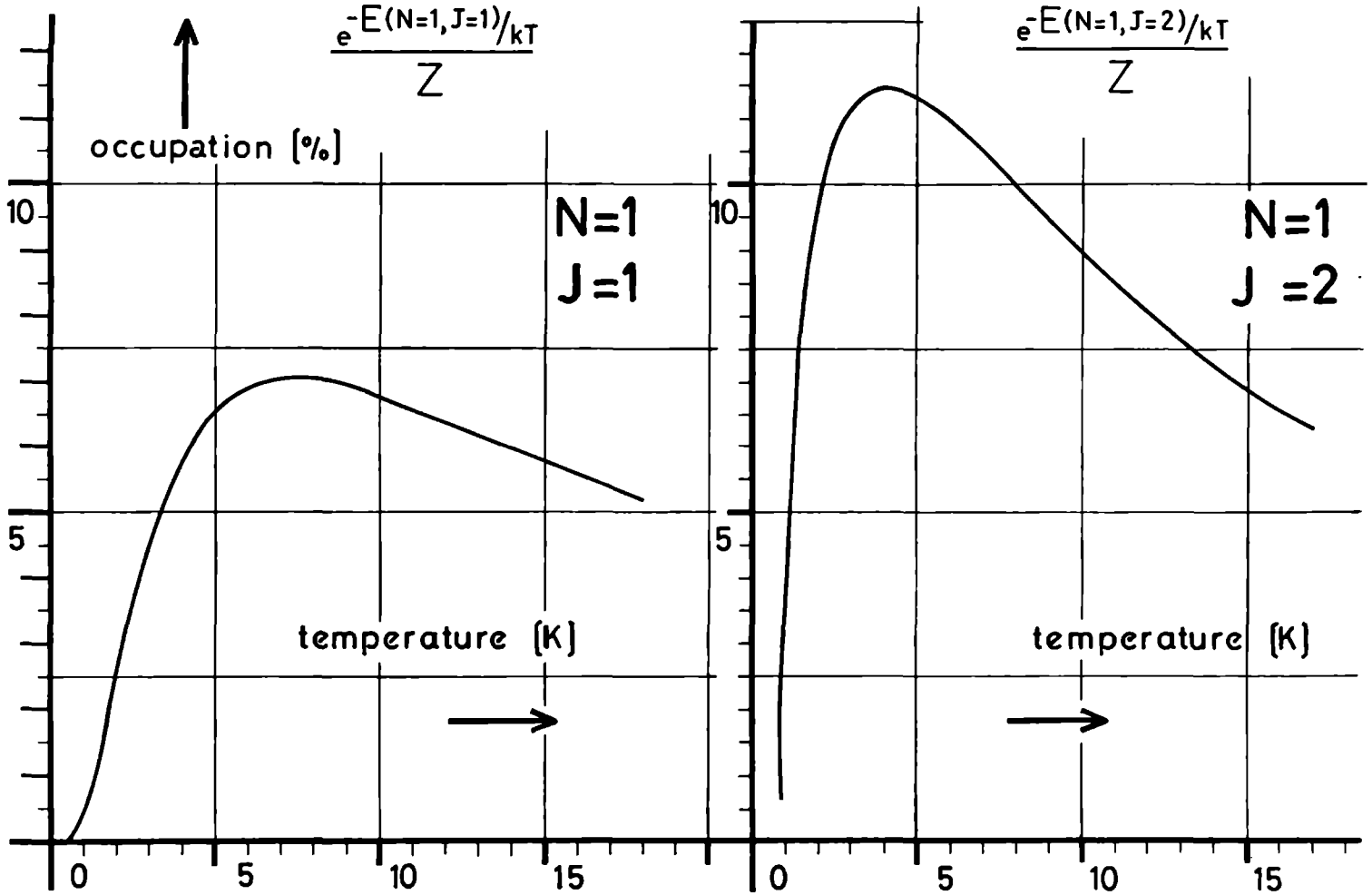

figures 2 and 3. Theoretical plot, occupation of (N=1, J=1) resp. (N=1, J=2) level.

for the degree of freedom considered. In certain cases some authors found a non-thermal behaviour within a single degree of freedom (e.g. rotation) [3,6,9,10,11]; for these, obviously, our method fails.

The result might be influenced by a varying velocity distributions of the beam for different P_0 values. To check on this point a mechanical velocity selector was used, and from the experimental results it was concluded that for O_2 molecules within the range of P_0 taken, the influence of a varying velocity distribution was well within the error of the temperature measurements. A sure way to avoid this effect, e.g. in case of polyatomic beam molecules, would be to select a certain velocity group of molecules during the measurements. A velocity selector also serves to avoid Mach number effects.

The magnetic-beam-resonance apparatus is shown in figure 4. Its main features will be described briefly. The molecular beam originates from a supersonic expansion through a nozzle of 100 μm diameter. At the other end of the machine the molecules are ionized by means of electron bombardment, then mass selected by a quadrupole mass filter and finally measured by a particle multiplier. Between the gas source and detector the state selecting and transition regions are located. These consist of the A, B and C fields. The A and B fields are Rabi-type deflecting magnets; the C field consists of a homogeneous magnet containing either a radio-frequency coil or a microwave cavity. Two slits are placed on the beam axis; the one 800 μm wide is placed inside the C field and the other 1600 μm wide is located at the detector entrance. The A and B magnets have opposite field gradients. The beam machine is operated in the flop-out mode [15]

In order to use phase-sensitive detection the molecular beam is modulated by one or other of two complementary techniques. One of these is with a mechanical beam chopper, which interrupts the beam periodically. The other uses amplitude modulation of the r.f. or microwave radiation. With the former method the total beam flow F is measured. The latter method is used to probe the change in intensity due to a given r.f. or microwave transition. The r.f. transitions (~ 40 kHz linewidth) are induced by the r.f. magnetic field of a coil of which the axis is coaxial with the beam; for the microwave transitions (~ 30 kHz linewidth), a compact, semi-open resonator is used. Details of the construction of this resonator are given in the appendix.

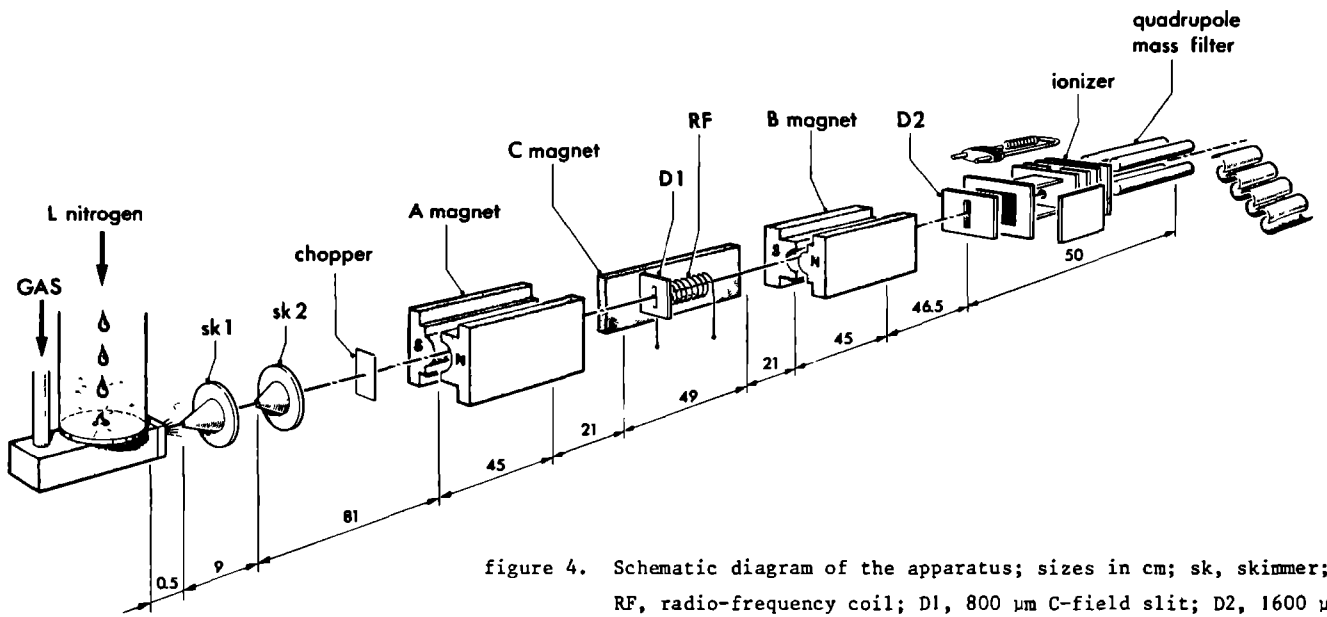

figure 4. Schematic diagram of the apparatus; sizes in cm; sk, skimmer; RF, radio-frequency coil; D1, 800 μm C-field slit; D2, 1600 μm detector slit. The microwave cavity can be exchanged for the RF coil shown.

APPLICATION OF THE METHOD TO THE O_2 MOLECULE IN THE GROUND STATE $^3\Sigma_g^-$

The O_2 molecule has no hyperfine structure because O^{16} has zero nuclear spin. The angular momentum N of the molecular rotation couples with the total electron spin S=1 to the final rotational quantum number J, with J=N,N±1. Because of the symmetry of the ground state ($^3\Sigma_g^-$) only odd N-states are occupied [16] Each rotational state is a triplet of which the lowest level is N=1, as shown in figure 5.

The beam temperature measurement was performed on O_2 using r.f. transitions within the nearly equally spaced multilevel system that occurs if a magnetic field $B_{dc} \lesssim 2$ m tesla is applied in the C-field region. For these magnetic transitions the selection rules are $\Delta J=0$ and $\Delta M_J=\pm 1$, assuming $\vec{B}_{r.f.} \perp \vec{B}_{dc}$. In "zero" magnetic field $\vec{B}_{dc}=0$ the allowed microwave transition N=1,J=1 ↔ N=1,J=2 was also used to confirm results with the r.f. measurements.

The results of the measurements are shown in figures 6 and 7, where the influence of the O_2 concentration in the seeding gas and of source temperature T_0 can be seen. The error in the temperature measurement depends on the accuracy by which the maximum of the function X and its half maximum values can be determined, as indicated in the results presented graphically. The temperature T actually determined is the spin temperature [17] describing the molecular population distribution within the triplet N=1; J=0,1,2.

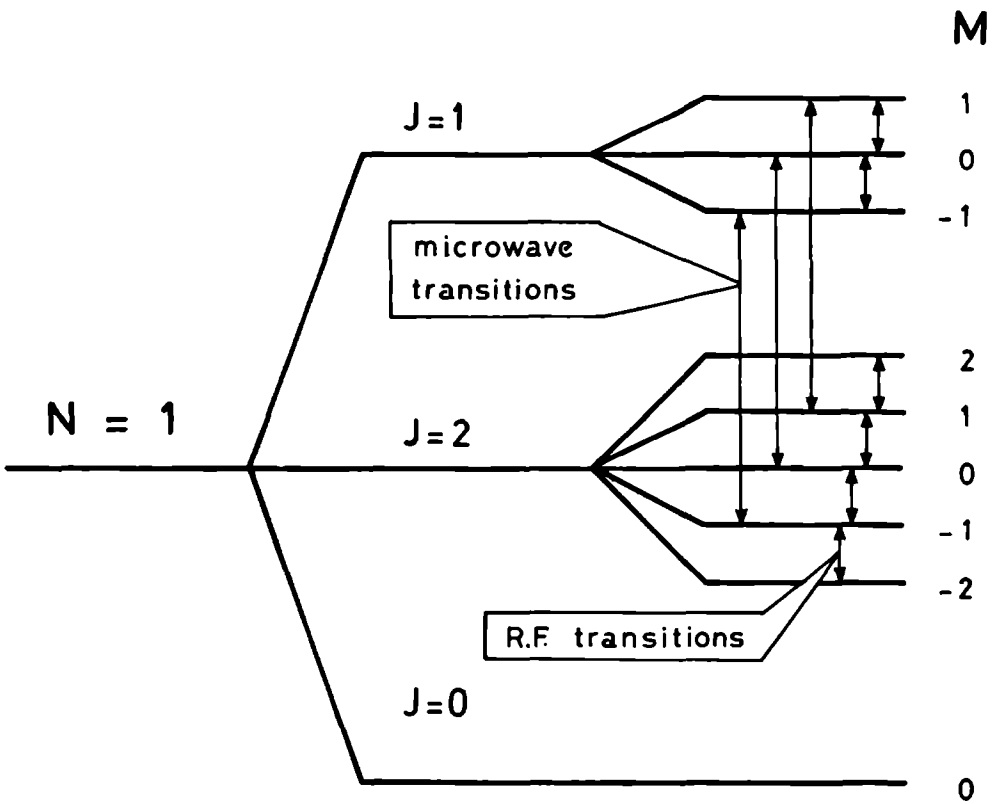

figure 5. Energy scheme of lowest triplet of $^{16}O^{16}O$, showing r.f. and microwave transitions.

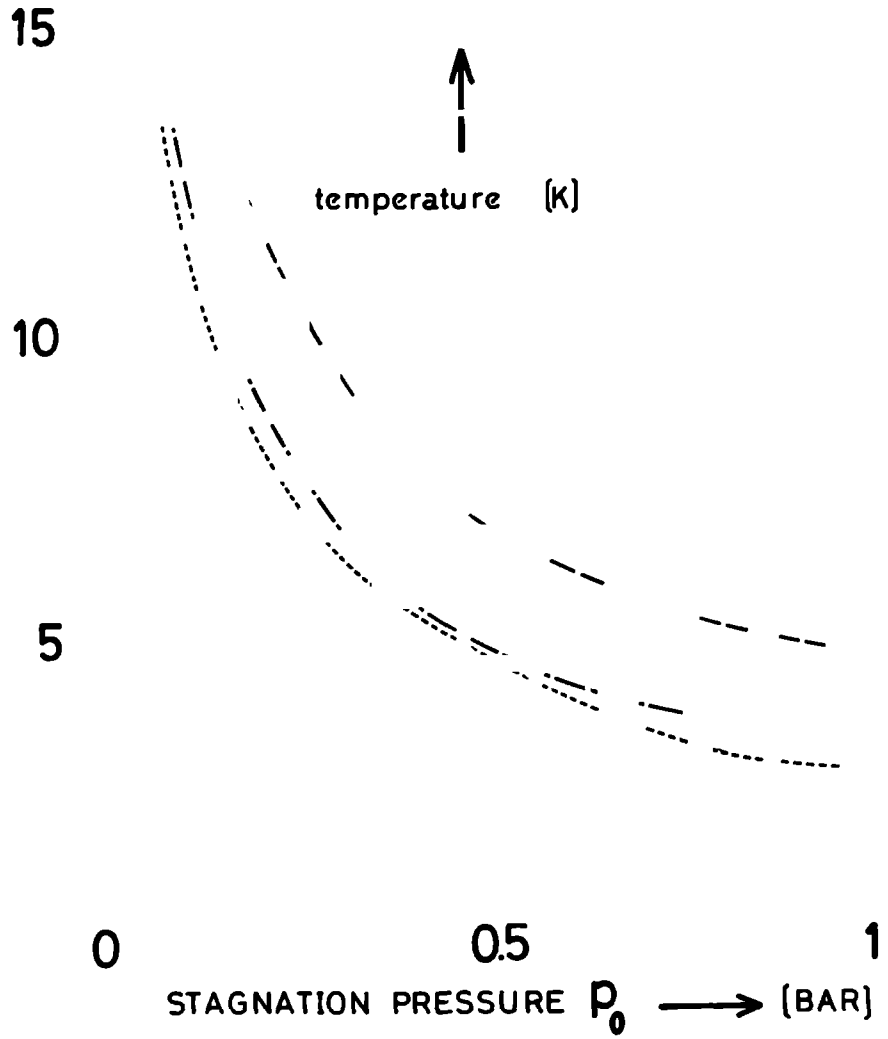

figure 6. Plot of relevant rotational beam temperature versus the stagnation pressure P_0.
Gas source at room temperature.

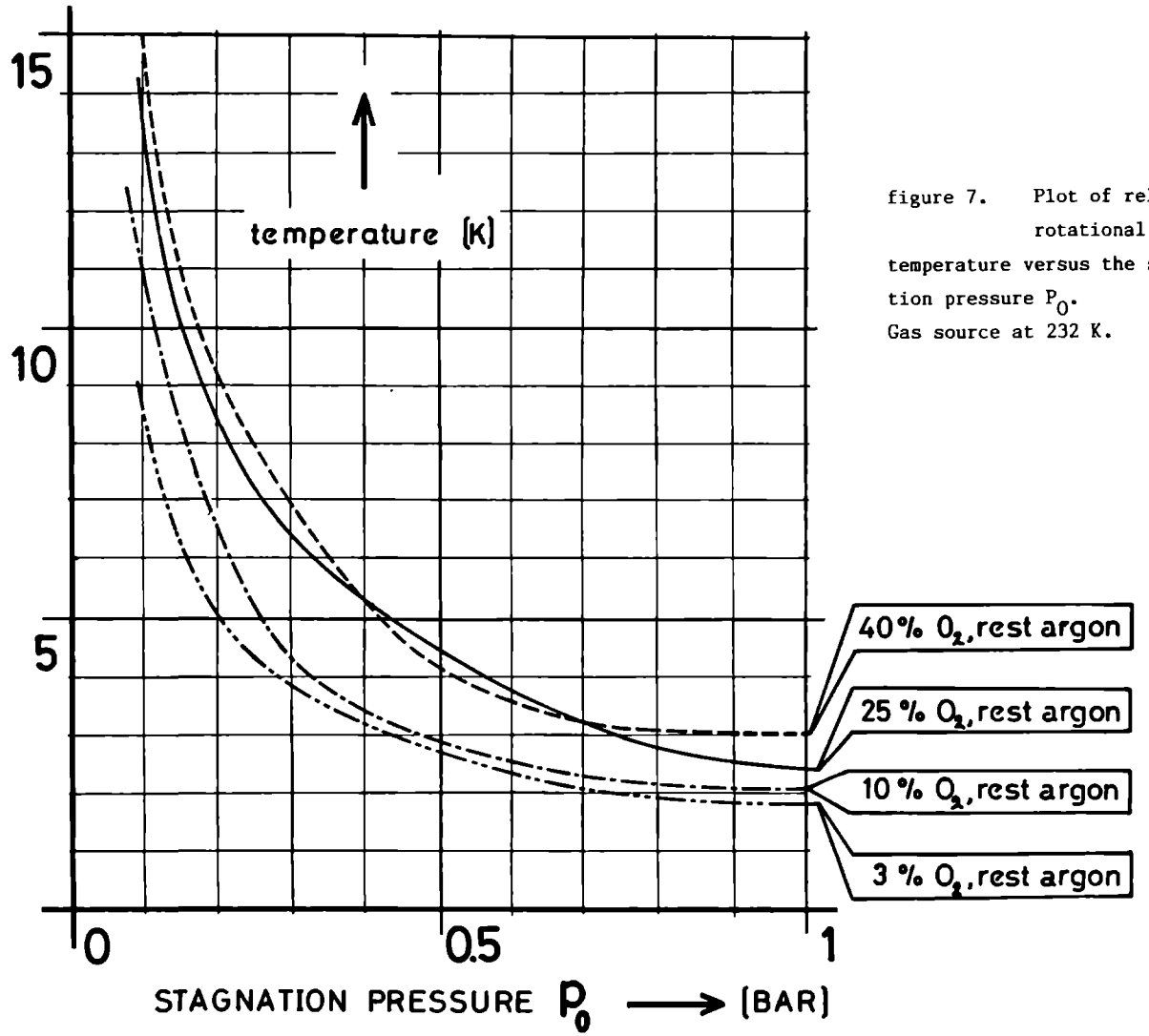

figure 7. Plot of relevant rotational beam temperature versus the stagnation pressure P_0.
Gas source at 232 K.

LIMITATIONS

There exist some limitations to the method. In principle, the population of a single state is compared to the total number of molecules. Consequently, the extraction of a temperature becomes dubious if non-equilibrium exists between the different degrees of freedom (e.g. rotational distribution, characterized by quantum number N and spin state distribution characterized by quantum number J for fixed N, in case of O_2). Because $\Delta E_N/k \approx 20$ K, for N=1 and N =3, and $\Delta E_J/k \approx 3$ K (assuming a typical splitting of 60 GHz), within 10% the O_2 temperature T determined by us corresponds to T_{rot} if $T \gtrsim 30$ K, and to T_{spin} if $T \lesssim 7$ K. Apart from this principal difficulty (elucidated for the specific case of O_2) four other limitations will be discussed.

Firstly, the probed level cannot be the ground state, because it does not possess a maximum of detected relative occupation as function of P_0, neither is there a Zeeman splitting in the case of O_2, therefore no r.f. transitions, although a microwave transition can be used. Similarly, levels very close to the ground state may assume their maximum at P_0 values which are too high to be realized in an experiment.

Secondly, if the probed level lies too far above the ground state, the maximum cannot be attained or only with poor accuracy because it occurs at very low P_0 values.

Thirdly, experiments based on microwave transitions may uncover a measurement problem because normally they probe the sum population of both of the levels involved (see figure 5). The uncertain machine detection efficiency of molecules for different levels makes the result of temperature determination rather unreliable (it should be noted that laser transitions would be free of this difficulty since the upper level is usually not populated).

Fourthly, the onset of clustering brings about the difficulty that the determination of the total flow F becomes contaminated by cluster fragments. For molecular beams showing clustering the method can be modified in a rather elegant way in order to circumvent this last

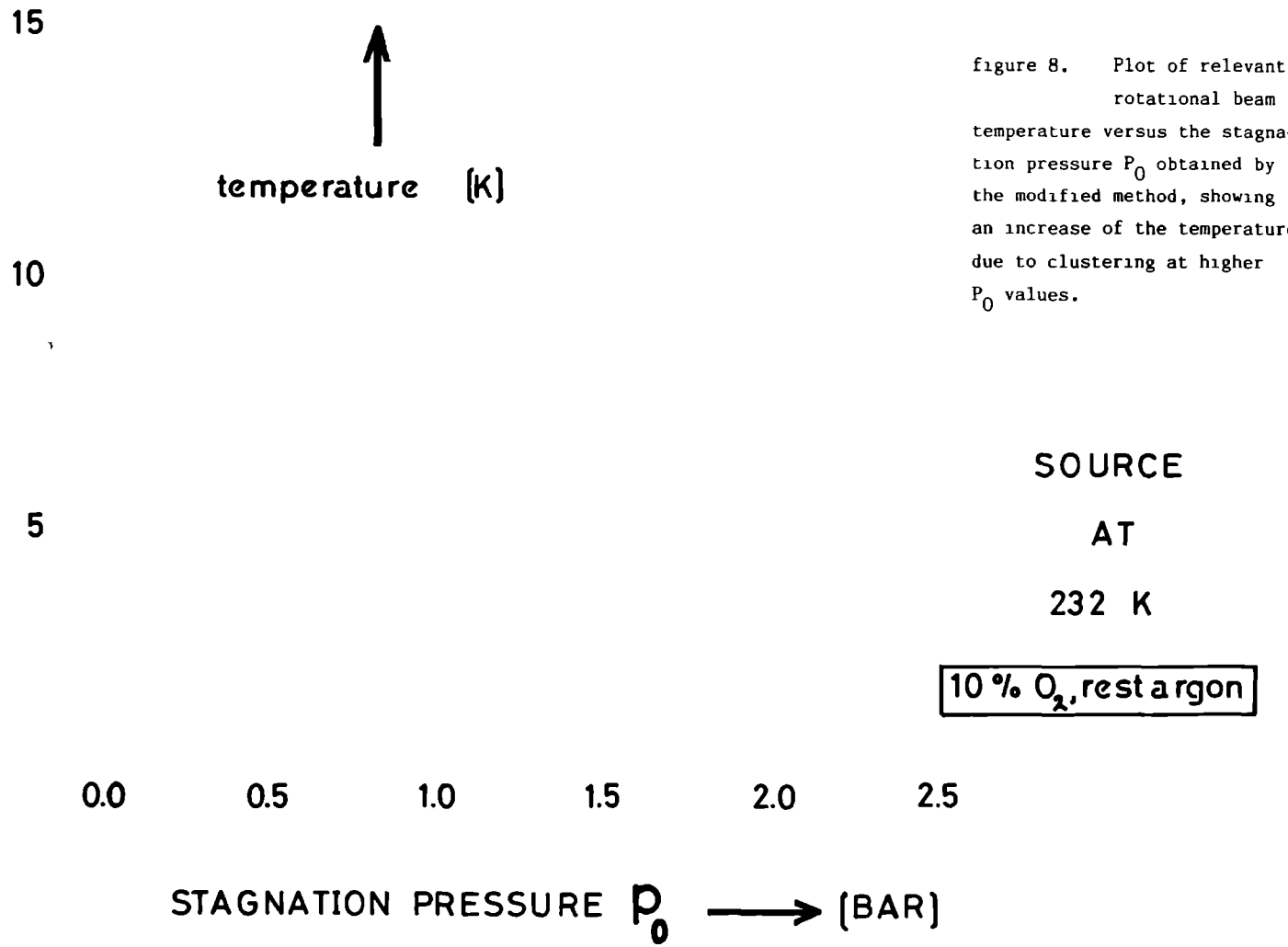

figure 8. Plot of relevant rotational beam temperature versus the stagnation pressure P_0 obtained by the modified method, showing an increase of the temperature due to clustering at higher P_0 values.

difficulty. In this case it is necessary to probe two independent levels, that is to determine $I_1(P_0)$ and $I_2(P_0)$. From the ratio I_1/I_2 as function of P_0 the temperature can be derived as before, using $\ln(I_1/I_2) = \text{const.} - (E_1-E_2)/kT$, but, note, without needing information on F. The constant term can be determined by the unmodified method at low P_0 values where no clustering occurs (see figure 8). Under the condition of the present experiments for which $P_0 \gtrsim 1$ bar, the temperature obtained by this modified method starts to increase rapidly with stagnation pressure, which is taken to indicate the onset of significant cluster formation.

Fifthly, an error can be introduced if high stagnation pressures are applied; beam broadening can change the efficiency of state selection by beam deflection, with respect to the total beam signal.
In contrast to all these limitations it should be mentioned that there is another advantage to the proposed method. Majorana flops are of little or no influence on the results because the fraction of affected molecules can be assumed to be constant.

The method described offers the possibility of an easy measurement of an internal beam temperature.
Results with the molecule O_2 show the expected lower beam temperature for mixtures with a lower O_2 percentage. Even under conditions of heavy beam condensation, a slight modification of the method allows a determination of the internal beam temperature; a significant rise for increasing P_0 values is observed.

For the 60 GHz microwave (magnetic) transition, a compact, semi-open resonator was constructed with an especially wide mechanical tuning range. A high Q value of 8700 permitted saturation of the microwave transition. Already for a klystron power of 50 mW, saturation has been achieved.

The O_2 results reported in this paper are in agreement with the spin temperature as determined by an independent method developed by Amirav et al [17] Two Raman measurements of the rotational temperature in an O_2 molecular jet, [5,18] yield values at nozzle distances $\lesssim$ 10 nozzle diameters; the lowest values reported are about 10 K. Taking into account that these values do not yet correspond to terminal ones of a complete expansion, see for instance [4], there is no contradiction with the lower values reported in the present paper. The first determination of T_{rot}, [19], yielded the terminal value of 30 K, for a 250 μm Ø nozzle and low stagnation pressure, P_o = 180 torr, in a pure O_2 beam.

Appendix: The semi-open mm-wave resonator

Although the cavity developed in the course of the experiment did not play the important role anticipated, we think it worthwhile to convey the experience gained.

The experimental requirements placed on a mm-wave resonator operating in the 60 GHz spectral region for use with oxygen molecules in a MBMR spectrometer are quite severe. Firstly, with an expansion cooled beam of oxygen, most of the spectral lines of interest lie between the frequencies of the 1^+ transition at 56.27 GHz, to the 3^- transition at 62.48 GHz. This spectral range contains all lines with N = 1 to 13 (N odd for $^{32}O_2$), with the exception of N = 1^- which lies at approximately 119 GHz. Thus the tuning range required is about 6.5 GHz. Secondly, since oxygen is strongly paramagnetic, the magnetic C-field of the spectrometer needs to be rather homogeneous to secure narrow spectral lines. This requirement limits the magnet gap width into which a tunable mm-wave resonator may be placed. Thus the resonator, together with its tuning mechanism must be particularly compact. Thirdly, the resonator must be sufficiently open in its construction to allow the molecular beam free passage through it, yet it must retain a high Q value so that the maximum transition probability for the oxygen transitions can be secured with mm-wave sources with a power output of 100 mW or less. Furthermore, the modes must be well spaced in frequency to avoid line distortion phenomena.

The type of cavity mode desired for MBMR spectroscopy is one for which a single maximum of the magnetic component of the radiation field exists along the beam trajectory. If more than one maximum is allowed, every spectral line is split into two by the longitudinal Doppler effect. Moreover, the type of mode employed and its configuration with respect to the field of the C-magnet will determine whether $\Delta M = 0$ or ± 1 transitions, or both, are excited. The requirements of a suitable mode together with high Q and wide tuning range have been met by the adaptation of the semi-open resonator of the type discussed by Krosta, [20] and by Legrand et al. [21] for bulk gas spectroscopy, to a miniaturized form suitable for molecular beam work.

A simplified diagram of the resonator is shown in Figure 9. It takes the form of a hybrid of a waveguide structure and a Fabry-Perot resonator in which one mirror is curved cylindrically, and the other plane. The waveguide structure comprises two conducting plates (which if suitably insulated electrically can also be used to form a Stark cell). The radiation field intensity is gaussian in a direction parallel to both the plane mirror and the molecular beam axis, and sinusoidal between waveguide flats, in the direction perpendicular to the beam. The lowest loss mode is TE_{10q} which is excited by a waveguide located in the flat mirror. The spatial field configuration for this mode relative to the quasi-static field B_{dc} of the C-field magnet is indicated in Figure 9. Since the radiation field B_{ac} has components both parallel and perpendicular to B_{dc}, Zeeman transitions corresponding to $\Delta M = 0, \pm 1$ may be expected to occur. The microwave magnetic field however, is a maximum at the beam, with B_{ac} parallel to B_{dc} so $\Delta M = 0$ occurs preferentially.

The general conditions of resonance and a discussion of other features of the TE_{nmq} mode cavity are given by Krosta [20]. In the cavity described below, n = 0, m = 0 and q, the longitudinal mode number, is either 4 or 5.

A brief account follows of the constructional details of the cavity based on the sketch shown in Figure 9. A pair of surface ground OFHC copper waveguide flats 6.3 x 25.3 x 40.2 mm were spaced 6.4 mm apart by a matched pair of blocks fabricated out of Corning machinable glass-ceramic. Holes were machined out of these blocks to give free passage of the molecular beam lengthwise through the cavity. The blocks were channelled on the inside to accommodate a fixed brass reflector at the bottom and a cylindrically curved brass reflector at the top. The latter reflector was made to slide freely up and down the guiding channels in the glass-ceramic blocks. The radius of curvature of the mirror was 180 mm. The distance between flat and curved mirrors could be adjusted within the limited headroom available by an eccentric drive shaft parallel to the longitudinal axis of the resonator, which was set to its angular position by a suitably geared shaft from outside the vacuum system. The channelling

of the glass ceramic used to locate the mirrors also provided electrical isolation between reflectors and waveguide plates. Whilst the Stark cell facility not used in the present work, it could be valuable in certain types of experiments. The waveguide was inserted into the mid-point of the flat resonator, thereby exciting the principal mode TE_{10q}, with q = 4 or 5. The coupling hole was drilled through a wall 0.5 mm thick of diameter 1.4 mm. In order to retain a high Q value, the cavity was undercoupled and gave a reflection coefficient of 0.3 when tuned to the principal mode TE_{10q}. This coupling served for the full tuning range required.

The cavity modes were explored by means of a thin sliver of paper inserted through the gap between waveguide flats and the sliding curved mirror. Movement of the sliver in a longitudinal direction at various depths produced visible variations of the cavity mode amplitude and freqency, when displayed on an oscilloscope, due to losses introduced via damping of the electric field component of the mm-radiation field within the resonator. The desired TE_{10q} mode was identified through the single reduction of cavity resonance amplitude as the paper sliver was moved from one end of the resonator to the other. Many other modes were also found, corresponding to 1, 3 and 5 E-field maxima along the resonator axis (modes TE_{1mq}, TE_{3mq}, ... m = 0, 2, 4 ..., q = 4 or 5).

The spatial extension of the radiation field in a longitudinal direction was also explored by the same method; in the present resonator the mean length of the effective interaction region was found to be about 25 mm.

Since the temperature coefficients of brass and machinable glass-ceramic used were in the ratio of 2 : 1 the differential thermal expansion of brass and glass-ceramic for the dimensions used was close to zero. The measured temperature coefficient of tuning was $\leq$ 300 kHz K^{-1}. Thus, thermal stabilization was not considered necessary.

The tuning as a function of spacing between resonator reflectors was 5.2 GHz mm^{-1}. Thus, by the use of the maximum permissible displacement in the

present design, a mechanical tuning range of 55-68 GHz was obtained for the principal mode TE_{10q}, which covered the full spectral range of interest. Fine tuning of 0 - 30 MHz was effected without serious degredation to the resonator Q ($\sim$ 8700 at 60 GHz), by applying pressure to the coupling waveguide, thereby flexing the nominally flat reflector.

When the resonator was used in the MBMR spectrometer in the lowest order mode, with optimal excitation for maximum signal a transit-time limited linewidth (FWHM) of $\sim$ 30 kHz at 56.27 kHz ($N = 1^+$ line) was obtained with a signal-to-noise ratio in excess of 50 : 1.

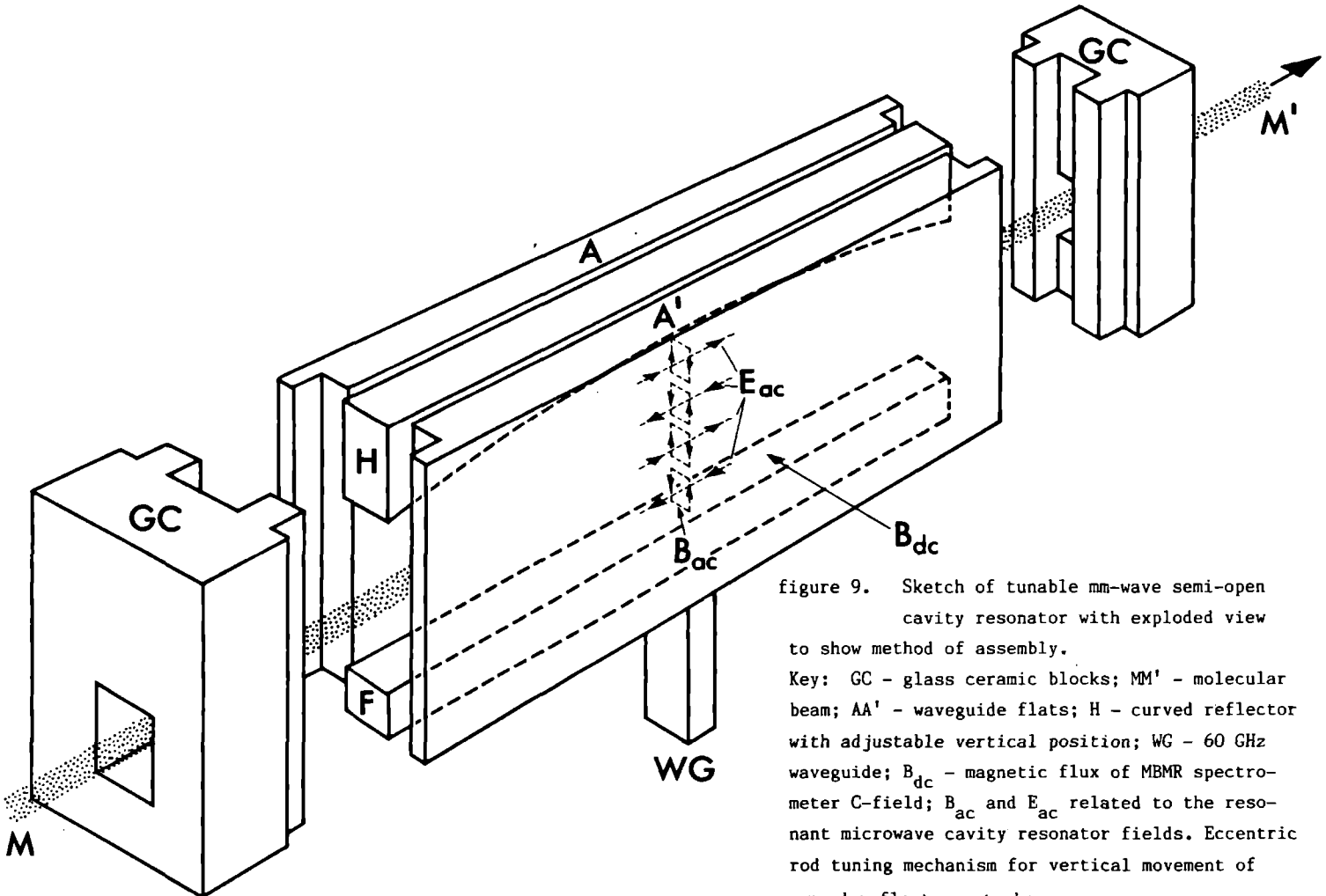

figure 9. Sketch of tunable mm-wave semi-open cavity resonator with exploded view to show method of assembly.

Key: GC - glass ceramic blocks; MM' - molecular beam; AA' - waveguide flats; H - curved reflector with adjustable vertical position; WG - 60 GHz waveguide; B_{dc} - magnetic flux of MBMR spectrometer C-field; B_{ac} and E_{ac} related to the resonant microwave cavity resonator fields. Eccentric rod tuning mechanism for vertical movement of curved reflector not shown.

ACKNOWLEDGEMENT

The authors are grateful for the technical support received at Nijmegen from messrs. C. Sikkens, L. Hendriks, F. van Rijn, J. Holtkamp, and H. Clephas for skilful assistance. Thanks are also due to Mr. E. Greasley at Keele for the development of the tunable microwave resonator. Finally acknowledgement is made of the financial support of NATO in the provision of a travel grant (grant no. 139.80) for one of us (Derek Lainé) which made this collaborative project possible, and the Stichting voor Fundamenteel Onderzoek der Materie (FOM) for supporting this project financially.

LIST OF REFERENCES

[1] W.L. Meerts, G. ter Horst, J.M.L.J. Reinartz and A. Dymanus
Chem. Phys. 35 (1978) 253

[2] P. Poulsen and D.R. Miller
Prog. Astronaut. Aeronaut. 51 (1977) 899
K. Winkelman, Rarefied Gas Dynamics
Proc. Int. Symp. 11 (1979) 899

[3] S.P. Venkateshan, S.B. Ryali and J.B. Fenn
J. Chem. Phys. 77 (1982) 2599

[4] G. Luijks, S. Stolte and J. Reuss
Chem. Phys. 62 (1981) 217

[5] H.P. Godfried,
Thesis (1982), Municipal University of Amsterdam

[6] R.E. Smalley, L. Wharton and D.H. Levy
J. Chem. Phys. 63 (1975) 4977

[7] P.J. Dagdigian
J. Chem. Phys, 64 (1976) 2609

[8] M. Faubel and E.R. Weiner
J. Chem. Phys. 75 (1981) 641

[9] D. Bassi, A. Bosschetti, S. Marchetti, G. Scoles and M. Zen
J. Chem. Phys. 74 (1981) 2221

[10] J. Verberne, I. Ozier, L. Zandee and J. Reuss
Mol. Phys. 35 (1978) 1649

[11] S.G. Kukolich, D.E. Oates and J.H.S. Wang
J. Chem. Phys. 61 (1974) 4686

[12] L. Zandee and J. Reuss
Chem. Phys. 26 (1977) 327

[13] J. Verberne and J. Reuss
Chem. Phys. 50 (1980) 137
Chem. Phys. 57 (1981) 189

[14] M. Waayer, M. Jacobs and J. Reuss
Chem. Phys. 63 (1981) 247, 257 and 263

[15] N.F. Ramsey, "Molecular beams"
Oxford University Press (1956)

[16] Mizushima, "The theory of rotating diatomic molecules"
John Wiley & Sons Inc. (1975)

[17] A. Amirav, U. Even and J. Jortner
J. Chem. Phys. 73 (1980) 4217

[18] P. Huber-Wälchi and J.W. Nibler
J. Chem. Phys. 76 (1982) 273

[19] R.J. Gallagher and J.B. Fenn
J. Chem. Phys. 60 (1974) 3487

[20] A. Krosta, "Realization d'un resonateur microonde plan-cylindrique entre conducteurs plan-paralleles".
Univ. Lille, France (1977), Doct. thesis, order no. 653

[21] J. Legrand, B. Segard, A. Krosta and B. Macke
Rev. Sci. Instr. 49 (1978) 256

Magnetic spectra of the dimer O_2Ar

J. Mettes*, B. Heijmen*, P. Verhoeve*, D.C. Lainé** and J. Reuss*

* Fysisch Laboratorium, Katholieke Universiteit
Toernooiveld, 6525 ED Nijmegen, The Netherlands

** Physics Department, University of Keele,
Keele, Staffordshire ST5 5BG, U.K.

ABSTRACT

MAGNETIC SPECTRA OF THE DIMER O_2Ar

With the magnetic beam resonance technique, magnetic r.f. transitions in weak fields (B=2.81 Gauss) have been measured for expansion cooled O_2Ar dimers. These dimers are T-shaped, due to the anisotropic forces forming a rotational barrier (20 cm^{-1}). Spin interactions yield four end-over-end rotational ladders, starting at 0 GHz, 39.6 GHz, 99.6 GHz and 111.8 GHz. The end-over-end B_R constant amounts to about 2 GHz, corresponding with an O_2-Ar distance of 3.71 Å. Only for the levels of the second ladder there are significant magnetic transition dipole moments which contribute to the observed spectrum. To measure the spectrum, particle counting techniques have been applied to render beam signals as low as 1 count/s significant. The experimental set-up, an assignment of the spectra and a best fit value for the rotational barrier, obtained from a simple analytical model, will be discussed.

The magnetic-beam-resonance apparatus shown in fig. 1 was used for the spectroscopic measurements on the paramagnetic system O_2Ar. The molecular beam originates from a room-temperature source by means of a supersonic expansion through a nozzle. We used the so-called Rabi setup containing a single r.f. coil located in the C-field region. The measurements were done in non-zero magnetic field in order to achieve a Zeeman splitting. When moderate magnetic fields are applied one obtains an equidistant multilevel-system with the possibility to make transitions within such a system (see ref.1 where similar transitions are used for spectroscopy on the para-magnetic molecule oxygen).

Molecules, which undergo a transition in the C-field region and thereby change their magnetic moment are flopped out of the molecular beam by virtue of the B-magnet yielding a beam-signal attenuation.

In order to measure phase sensitively we can dispose of two modulation schemes. One technique employs a mechanical beam chopper, which interrupts the beam periodically; the other technique uses amplitude modulation of the r.f. radiation. With the former method one measures the total beam; it is used to optimize the molecular beam. The latter method only involves those molecules which make an r.f. transition and is used for spectroscopic purposes. The possibility to supply a noise-broadened high-power r.f. signal to the C field coil appeared to be very useful. Many possible transition frequencies of the r.f. spectrum are irradiated simultaneously and yield transitions starting from different initial states. The beam attenuation caused this way, is a good tool to check the conditions for spectroscopic measurements. Normally (without noise-broadening) one obtains a spectrum that rises out of the noise after many hours of measuring. At the detector arrive 150 counted O_2Ar dimers per

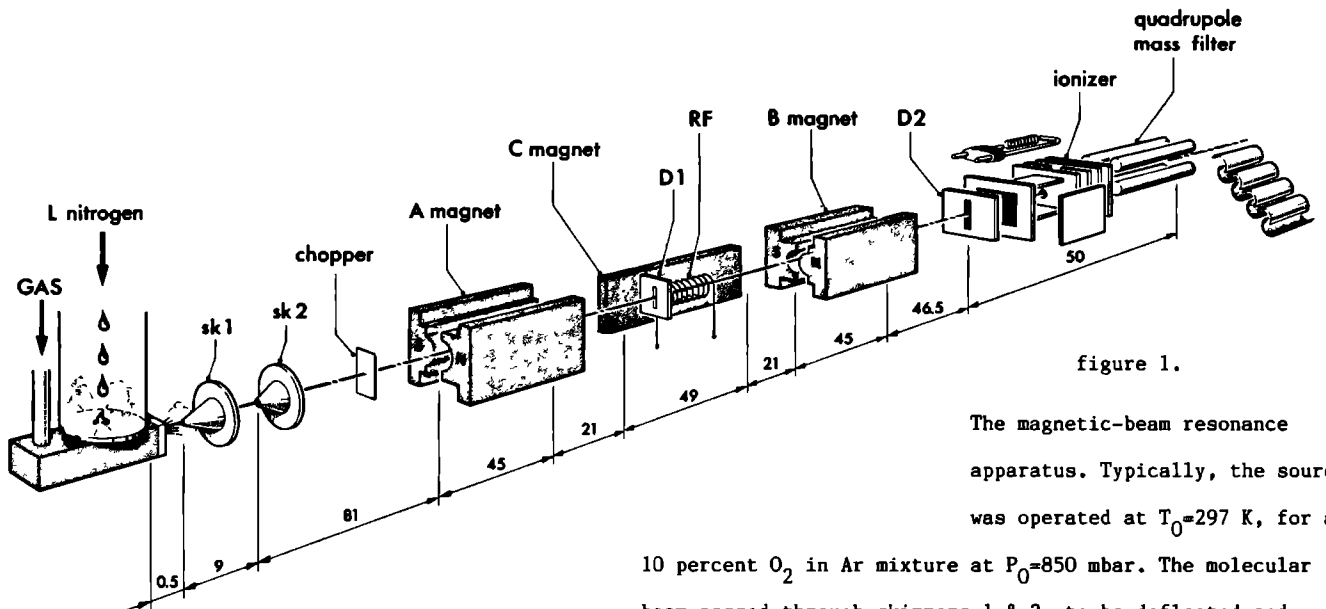

figure 1.

The magnetic-beam resonance apparatus. Typically, the source was operated at T_0=297 K, for a 10 percent O_2 in Ar mixture at P_0=850 mbar. The molecular beam passed through skimmers 1 & 2, to be deflected and redeflected by the A- and B-magnet. The collimators D1 (800 μm wide) and D2 (1600 μm wide) define the molecular beam width. At the detector, the beam height amounted to 8 mm. In the transition region, a magnetic rf-field along the beam axis and a DC-field perpendicular to it were applied. Detection was effected by an electron bombardment ionizer (electron energy 100 eV) followed by a quadrupole mass filter. The indicated distances are in cm.

second (detected on the O_2Ar^+ mass). From this amount we are able to detect attenuations as small as 1 count per second as a significant signal (1 hour/channel).

We also tried to do spectroscopy on O_2Ar with an Electric Beam Resonance machine but failed to focus the beam as the negative Stark-effect dominates. Our prognosis of the electric focussability of O_2Ar (estimated electric dipole moment 4 mD, see theoretical section) probably was too optimistic; other experiments on CH_3D and CH_3CD_3 with a supposedly equally weak dipole-moment have been succesfully performed on this machine, however (2,3).

The theory consists of two parts. First, a numerical approach (4) using a semi-empirical potential in a space fixed coordinate system yields energy-levels, Zeeman-splittings and the partition function for different temperatures. The partition functions enabled us to estimate the order of magnitude of the signals to be expected, under the assumption that the temperature of the dimers is equal to the temperature of the O_2 in the beam (for measurements of the oxygen temperature of the beam, performed with a novel method, see ref.5). Secondly, an analytical approach has been developed based on perturbation theory and using a body-fixed coordinate system (z-axis lying along the O_2-Ar axis); analytical expressions for the energy levels were obtained which contain 2 dimer parameters, the oxygen-argon rotational constant B_R and the rotational barrier V_2, both averaged over the groundstate, see ref.6. This model has been extended hereafter with the Zeeman terms leading to an analytical expression of the Zeeman-spectrum as a function of V_2.

A multiproperty analysis has been performed by Pirani and Vecchiocattivi (10)

resulting in a semi-empirical potential for the system O_2-Ar of the form $V_0(R) + V_2(R).P_2(\cos\theta)$, where θ is the angle between $\bar{R}$ and $\bar{r}$. The vector $\bar{R}$ connects the O_2 mass centre with the argon atom, the vector $\bar{r}$ connects the two oxygen atoms. In our opinion, the physical backing for this potential is so much superior that we refrained from discussing preceding attempts. Confrontation with the present experiment leads us to propose a modification of the $V_2(R)$-part of the intermolecular potential, at R-values around the minimum position of the $V_0(R)$-part; the $V_2(R)$-part is still strongly repulsive there, causing the O_2-Ar system to form a T-shaped structure (11).

EXPERIMENT; the MBR machine

The magnetic-beam-resonance apparatus (figure 1) will be described briefly. The molecular beam expands from a nozzle of 150 μm diameter. At the other end of the machine the molecules are ionized by means of electron bombardment, then mass selected by a quadrupole mass filter (tuned to O_2Ar^+) and finally measured by a particle multiplier. Between the gas source and detector the state selecting and transition regions are located. These consist of the A,B and C fields. The A and B fields are Rabi-type deflecting magnets (radius of the convex-,concave pole piece 4.68 mm resp. 5.51mm, leaving an opening of 3.8 mm and yielding a gradient of 5 kG/cm under typical working conditions); the C field consists of a homogeneous magnet containing a radio-frequency coil. Two slits are placed on the beam axis; the one 800 μm wide is placed inside the C field and the other 1600 μm wide is located at the detector entrance. The A and B magnets have opposite field gradients. The beam machine operates in the flop-out mode (7).

A beam-stop, mounted on the beam axis just before the first deflecting magnet (A magnet), is used for a dual purpose; it prevents the argon to enter the ultra high vacuum chambers (argon is hard to pump with ion getter pumps); further, it stops large clusters like $O_2(Ar)_n$, $n>>1$, which might fragment in the ionizer to the O_2Ar mass and contribute to the noise of the dimer signal.

Particle counting is applied, yielding a maximal signal to noise ratio because influence of electronic noise, drift etc. are handled optimally. Moreover, fluctuations in the multiplier current do not contribute anymore. The

fluctuation of the number of particles counted per time unit has been reduced to the statistical fluctuation of the number of particles involved, excluding disturbances like the ones discussed hereafter.

Theoretically, there is no limit to the improvement of signal to noise ratio obtained by the use of a transient recorder (S/N improves with the square root of the recording time), provided that the character of the fluctuations of the signal is purely statistical. In practice, we observe big disturbances that occur about three times per hour, appearing randomly in the spectra with amplitudes bigger than the signal gained after hours of averaging. This leads to non reproducible recording.
Using the fact that such disturbances are easily recognizable we have written a computer program to remove them from the collected data. We are left with statistical noise and continue to gain signal to noise by measuring longer. This is limited only by the patience of the experimentalist or break-down of the machine.

The choice of optimum source conditions is based on two factors;
a/ A maximum ratio between the deflectable part of the total beam signal S measured on O_2Ar^+ and the noise N of this signal.
b/ A minimum temperature of the O_2 monomers in the beam (see ref.5 for these temperature measurements) In fact one wants a minimum temperature of the O_2Ar clusters in the beam. It turns out that the O_2Ar temperature is roughly the same as the O_2 monomer temperature. The purpose of low temperature is to have a high population of only a limited number of low-energy states of O_2Ar. For the influence of the temperature on the partition function see ref.4.
The procedure followed has been to choose the conditions to get the lowest

temperature within the region of maximal S/N, see figure 2. For a 10 percent O_2 in argon mixture the optimum is reached at a stagnation pressure P_0=850 mBar and a room-temperature source, yielding a mixed dimer to O_2-monomer ion-ratio of 10^{-5}.

The homogeneous C magnetic field is calibrated by recording the Zeeman spectrum of O_2 molecules. A spectrum recorded this way is shown in the figure 3. A number of O_2 lines, see ref 1. for the identification, with known splittings yields the magnetic field strength.
Different field strengths are applied to check the linearity of the Zeeman effect. Fig.4.shows a part of the spectrum at a higher B field (together with low B). The observed structure reproduces after scaling.

We have also tried to measure an electric transition that is calculated to be at low frequency, 16 MHz, in zero B-field. For this purpose a parallel plate capacitor was inserted in the C field region in such a way that the E field component of the r.f. field, resulting from an AC voltage on the capacitor was perpendicular to the DC magnetic C field. Thus $\Delta|M| = 1$ transitions become allowed, the type of transitions detectable with our machine(a change of magnetic moment is necessary).
The electric transition dipole is proportional to the permanent electric dipole. An estimate of this permanent electric dipole moment of O_2Ar gave the value of 3 mD, a moment induced in the argon by the quadrupole moment of the O_2 ($\alpha Q\langle R^{-4}\rangle$; α=1.64Å^3 is the polarizability of argon; $Q=-0.39\times10^{-26}$ esu.cm^2 is the quadrupole moment of O_2 ; R=3.71 Å is the estimated distance between O_2 and Ar). We failed to see this electric line.

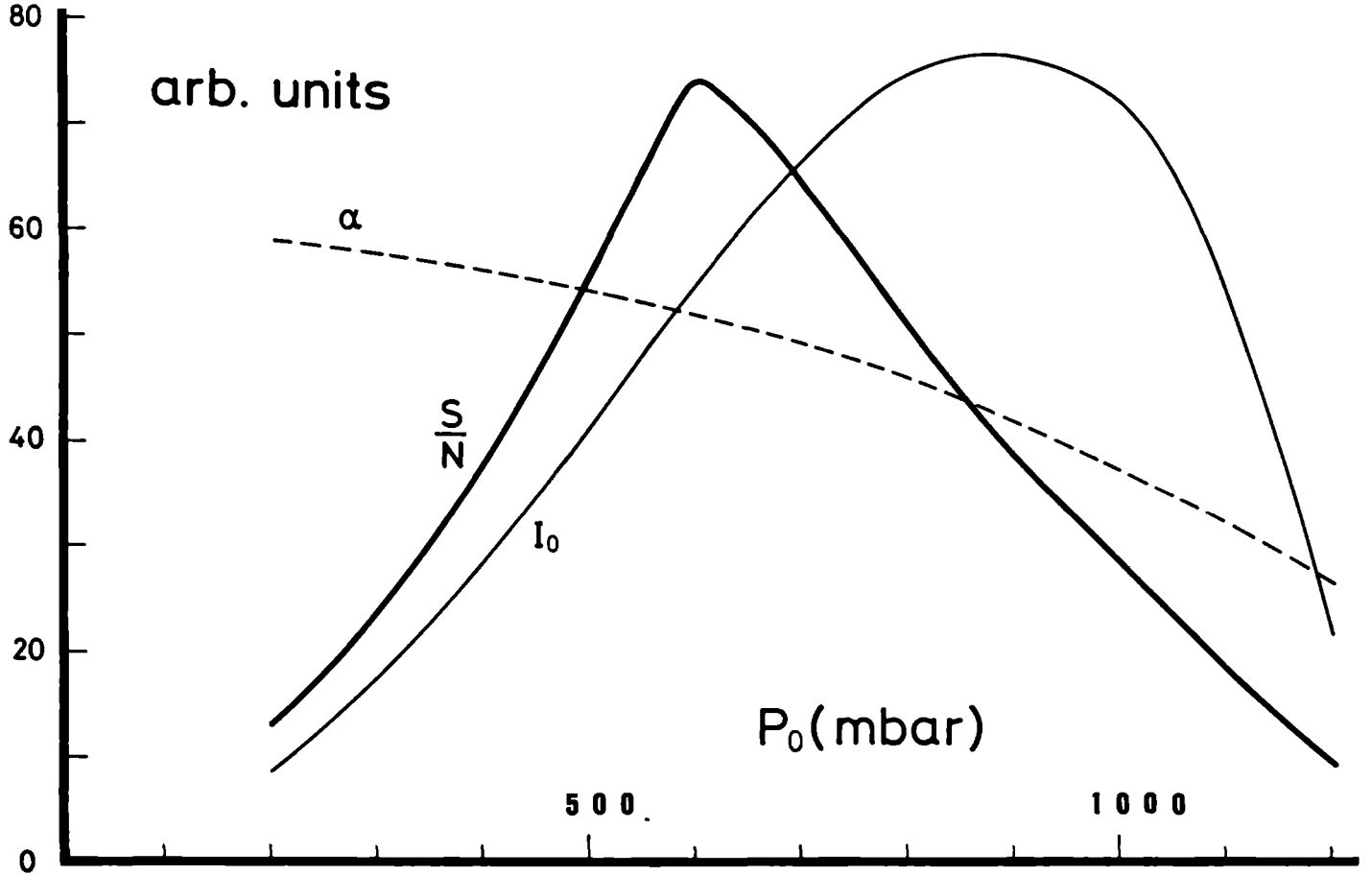

Figure 2. The choice of the optimum source conditions. Total beam signal on O_2Ar^+ (I_0), signal to noise ratio (S/N) and deflectable fraction (α) of this signal versus source pressure (P_0). For I_0, S/N and α the value 60 on the ordinate corresponds to about 100 counts-sec., 6 (3 sec time-constant of the lock-in amplifier) and 60 percent respectively. The source temperature was kept at T_0=297 K, for a 10 percent O_2 in Ar mixture.

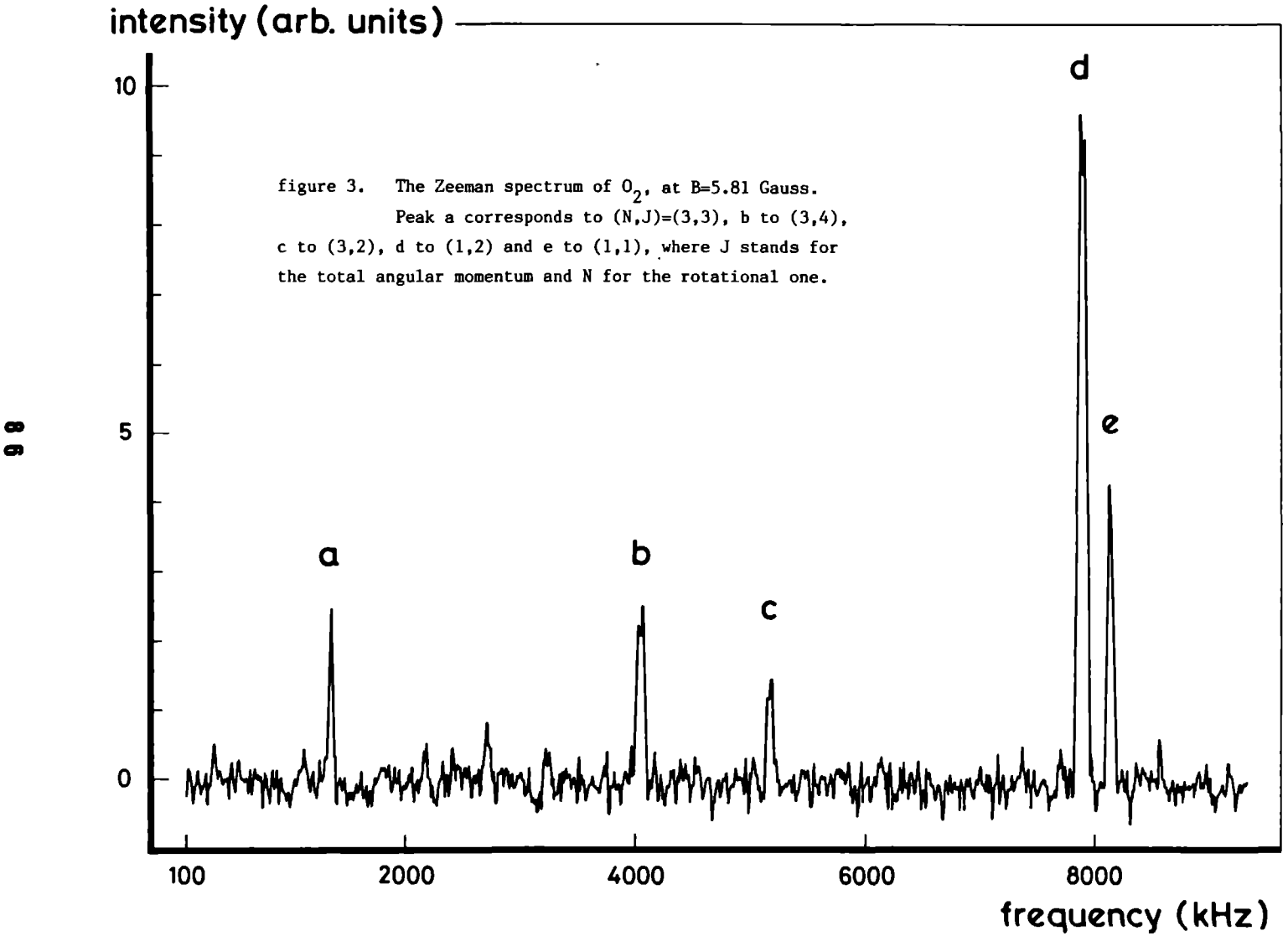

figure 3. The Zeeman spectrum of O_2, at B=5.81 Gauss. Peak a corresponds to (N,J)=(3,3), b to (3,4), c to (3,2), d to (1,2) and e to (1,1), where J stands for the total angular momentum and N for the rotational one.

As mentioned in (4), we originally intended to measure the fine structure spectrum of O_2Ar. A 60 GHz microwave cavity was constructed for this purpose. The succesfully obtained r.f. Zeeman-spectra, however, rendered this measurement unnecessary.

THEORY; the numerical and the analytical approach in general.

As mentioned in the introduction the interpretation of the Zeeman spectrum rests on two different approaches.

The numerical approach is outlined in ref 4.
Ro-vibrational calculations are performed on O_2Ar, taking into account coupling with the O_2 electronic spin. Two different empirical potentials are used and they give similar fine-structure spectra (in case of transitions in zero magnetic-field the selection rule is $\Delta F=0,\pm1$; because magnetic transitions are concerned there should be no change in parity). The anisotropy in the O_2Ar potential, $V_2(R)P_2(\cos\theta)$, is found to strongly perturb the O_2 fine-structure spectrum suggesting that the O_2Ar fine-structure spectrum and the Zeeman-spectrum can give detailed information about the anisotropy of the van der Waals interaction potential. Transition strengths for the fine-structure transitions are calculated and found to vary by two orders of magnitude.
The transition frequency of the previously mentioned electric (parity changing) transition is calculated to be 16.2 MHz (between the the states F=2, p=+ , 51.3764 GHz from the ground-state and F=2, p=-, 51.3926 GHz).
Coupled spherical harmonics and spinfunctions of the form $|((NS)JL)FM_F>$ were taken as angular basis functions; $|NM_N>$ represents the O_2 rotation (N must be odd) and $|SM_S>$ the angular momentum of the spin, for the ground state S=1. These two couple to $|JM_J>$, where J and M_J are the total angular momentum quantum numbers in case of pure O_2 (8). In the dimer $|JM_J>$ couples with $|LM_L>$, representing the end-over-end rotation of

the complex. Here, the total angular momentum is described by F and M_F. All M-quantum numbers (M_N,M_S,M_L and M_F) are taken here in a space-fixed coordinate system.

The linear Zeeman splitting of the levels is calculated, too, see table 1. The Zeeman hamiltonian $H = -g_e \mu_b \bar{S}.\bar{B}$ is responsible for this splitting, where μ_b is the Bohr magneton (1.39961 MHz/Gauss) and g_e is 2.00232 ref.8.

The analytical approach, discussed hereafter, forms an extension of the work of Van der Avoird (6). For the rotation-vibration-spin states in O_2-rare gas atom complexes a simple model is presented, which predicts the form of the fine-structure spectrum. The model contains two parameters due to the O_2Ar complex; the vibrational ground state average of the anisotropic potential V_2 and the end-over-end rotational constant B_R. Adjusting these parameters yields quantitative agreement with the energy levels obtained from the numerical dynamical calculations (4).

The parameters V_2 and B_R play a key role in the discussion hereafter. They stand for matrix elements

$V_2 = (h.c)^{-1} \langle i,p,F,M_F,vib | V_2(R) | i,p,F,M_F,vib \rangle$

and $B_R = \hbar^2 (h.c)^{-1} \langle i,p,F,M_F,vib | (2\mu R^2)^{-1} | i,p,F,M_F,vib \rangle$

The symbol "vib" indicates the Van der Waals stretch vibration (coordinate R); μ stands for the reduced mass. The values of V_2 and B_R depend on the eigenfunctions over which the expectation values are taken. In contrast to (11), we only consider the ground state of the Van der Waals stretch oscillation, thereby obtaining a value for V_2 (1165 GHz, theoretical value from the potential of (10), see below) which is larger than that obtained in (10) (500 GHz) from a Boltzmann distribution over all states, at T=93 K. The

experimentally determined average value (11), at 93 K, is 600±100 GHz. The positive value of V_2 reflects that the zero of the function $V_2(R)$ occurs at an intermolecular distance larger than the minimum distance of the isotropic part of the potential $V_0(R)$ (fig. 5).

The large positive value of the matrix-element V_2 causes the T-shape structure of the O_2-Ar complex.

Actually, for V_2 and B_R the values quoted by us slightly depend on the quantum numbers i and F.Within the potential model of (10) and using the "exact" eigenfunctions of the numerical approach (4) we find a variation of about 5 GHz around V_2=1165 GHz, for the different F-levels of the four i-ladders, with F<4. The B_R-value thus obtained shows a variation of about 0.02 GHz around the average of 2.08 GHz.

Alternatively the energy levels calculated by the numerical approach (4) were used to fit directly the value for B_R. One reproduces the rotational spacing within 1 percent for V_2>800 GHz and 1.97 GHz≤B_R≤2.07 GHz.

table 1. Zeeman splittings in kHz for a magnetic field of B=2.81 Gauss obtained by the numerical approach, for the potential of (10). The states are characterized by their total angular momentum F, their p parity and the ladder i=1,2,3 or 4 to which they belong. Measured values are given between brackets, for F=2 and F=3 the experiment gives averaged values of the even and odd transitions.

F p i	frequency		F p i	frequency	F p i	frequency
1 - 2			6 - 1	349.8	11 - 2	503.3
1 - 3	2234		6 - 2	647.2	11 - 3	222.1
1 - 4	2225		6 - 3	631.1	11 - 4	607.6
1 + 1	294.2		6 + 2	801.4	11 + 1	401.8
1 + 2			6 + 3	533.5	11 + 2	211.4
1 + 3	281.5		6 + 4	972.2	11 + 3	491.8
2 - 1	300.5		7 - 2	704.7	12 - 1	402.3
2 - 2	2829		7 - 3	436.3	12 - 2	168.9
2 - 3	606.6	(2819)	7 - 4	868.3	12 - 3	467.3
2 + 2	2850		7 + 1	364.7	12 + 2	472.7
2 + 3	1496		7 + 2	514.7	12 + 3	192.6
2 + 4	1825		7 + 3	603.2	12 + 4	565.1
3 - 2	1670		8 - 1	378.3	13 - 2	446.0
3 - 3	1101		8 - 2	412.3	13 - 3	168.5
3 - 4	1510	(1624)	8 - 3	574.3	13 - 4	
3 + 1	310.0		8 + 2	635.1	13 + 1	399.4
3 + 2	1622		8 + 3	362.1	13 + 2	135.1
3 + 3	667		8 + 4	784.1	13 + 3	444.3
4 - 1	321.3		9 - 2	581.8	14 - 1	393.8
4 - 2	1111	(1093)	9 - 3	304.3	14 - 2	108.4
4 - 3	671.3		9 - 4	715.0	14 - 3	
4 + 2	1193	(1168)	9 + 1	389.6	14 + 2	422.3
4 + 3	843.1		9 + 2	330.5	14 + 3	148.6
4 + 4	1278		9 + 3	545.6	14 + 4	
5 - 2	947.3	(924.6)	10 - 1	397.5	15 - 2	401.0
5 - 3	663.8		10 - 2	264.6	15 - 3	
5 - 4	1104		10 - 3	518.1	15 - 4	
5 + 1	335.0		10 + 2	539.0	15 + 1	386.2
5 + 2	830.5		10 + 3	258.7	15 + 2	
5 + 3	655.4		10 + 4	657.0	15 + 3	

In the tables 2a & 2b the energy matrices (including a Zeeman term) are displayed, for O_2Ar. In principle, the basis of the first order model (6) has been used,

$$|1\rangle = \frac{1}{\sqrt{2}} \left(|1,1;1,-1;0,F,M_F\rangle + |1,-1;1,+1;\ 0,F,M_F\rangle \right)$$

$$|2\rangle = \frac{1}{\sqrt{2}} \left(|1,1;1,+1;2,F,M_F\rangle \pm |1,-1;1,-1;-2,F,M_F\rangle \right)$$

$$|3\rangle = \frac{1}{\sqrt{2}} \left(|1,1;1,\ 0;1,F,M_F\rangle \pm |1,-1;1,\ 0;-1,F,M_F\rangle \right)$$

$$|4\rangle = \frac{1}{\sqrt{2}} \left(|1,1;1,-1;0,F,M_F\rangle - |1,-1;1,+1;\ 0,F,M_F\rangle \right)$$

The kets $|N,M_N;S,M_S;K,F,M_F\rangle$ contain the body-fixed quantum numbers M_N, M_S and K. Within this basis, the spin interaction (spin-spin & 2nd order spin-orbit, eq. 17, ref.6) is diagonalized; similarly, the diagonal term of the Coriolis-interaction is taken into account in the determination of the first order energy levels, yielding

$$\varepsilon_1^{(1)} = B_R F(F+1), \qquad \varepsilon_2^{(1)} = B_R F(F+1) + \frac{4}{5}\lambda_0 - 4B_R,$$

$$\varepsilon_3^{(1)} = B_R F(F+1) + \frac{6}{5}\lambda_0, \qquad \varepsilon_4^{(1)} = B_R F(F+1) + \frac{8}{5}\lambda_0$$

The p-parity of the states is even for $|1\rangle$ and odd for $|4\rangle$; the states $|2\rangle$ and $|3\rangle$ are parity-degenerate possessing even and odd parity. For each parity, we have a 3x3 energy-matrix. Including the end-over-end rotation, the total parity becomes $(-)^{p+F+1}$ (6). To get some feeling for the actual energy values one has to consider the rotational constant B_R=2.097 GHz, for the end-over-end rotation, and λ_0=59.5 GHz for the spin-interaction constant.

The first order results have to be corrected, in two ways. The diagonal values are strongly perturbed by spin-spin-admixture of N=3 eigenfunctions and the N=1, M_N=0 eigenfunction; also the anisotropic potential term V_2 couples

the N=3 eigenfunctions to the first order states $|i>$, i=1,..,4. As shown in ref.6, the energy shifts $\epsilon_i^{(1)} \rightarrow \epsilon_i = \epsilon_i^{(1)} + \epsilon_i^{(2)}$ are considerable although the amplitude of the admixed states remains small so that perturbation theory still yields good results. Accordingly, we use the perturbed ϵ_i-values for which analytical expressions can be found in ref.6, as function of λ_0 and V_2.

The second correction results from the Coriolis-interaction (eq. 16, ref.6) which couples states with K-values differing by one. In the matrices (tables 2a & 2b) this interaction is represented by off-diagonal terms containing B_R. As a consequence, the p-degenerate levels $|2>$ and $|3>$ split. We discuss this Coriolis-effect together with the Zeeman effect.

The Zeeman-terms (ZT) derive from the operator

$2\mu_B B \hat{S}_Z^{SF} = 2\mu_B B \sum_{\nu=0,\pm1} D^{1*}_{0\nu}(\alpha,\beta,0)\, S_\nu^{BF}$ concerning the rotation matrix elements we keep to the convention of Brink and Satchler, ref. 8. The symbol B is used for the magnetic field strength; μ_B stand for the Bohr-magneton (μ_B/h = 1.39961 MHz/Gauss). The superscripts SF and BF are used to indicate Space-Fixed and Body-Fixed operators, respectively. The diagonal-elements of tables 2a & 2b are calculated with the help of

$$<N,M_N;S,M_S;K,F,M_F\ |ZT|\ N,M_N;S,M_S,K,F,M_F> =$$

$$2\mu_B(2F+1)\begin{pmatrix} F & 1 & F \\ M_F & 0 & -M_F \end{pmatrix}\begin{pmatrix} F & 1 & F \\ K & 0 & -K \end{pmatrix}|M_S|\ (-)^{-M_F-K} \qquad \text{eq. 1}$$

From eq.1 follows $<3|ZT|3>=0$ because of $|M_S|=0$, and $<1|ZT|1>=<4|ZT|4>=0$ because 1+F+F= odd and K=0, i.e. $\begin{pmatrix} F & 1 & F \\ 0 & 0 & 0 \end{pmatrix} = 0$. For the only non-zero diagonal terms one has;

$$<2|ZT|2> = 4\mu_B B \frac{M_F}{F(F+1)}$$

The off-diagonal terms are calculated from

$$\langle N,M_N';S,M_S';K',F,M_F|2\mu_B\ B\ \hat{S}^{BF}_{\pm1}\ D^{1\ *}_{0\ \pm1}(\alpha,\beta,0)|N,M_N;S,M_S;K,F,M_F\rangle\ =$$

$$\delta_{M_N',M_N}\ \delta_{M_S',M_{S\pm1}}\ (-)^{1-M_F-K}\ \mu_B\ B\ \frac{1}{\sqrt{2}}\ \sqrt{(S(S+1)-M_S(M_S\pm1)}\ (2F+1)\begin{pmatrix}F & 1 & F\\ M_F & 0 & -M_F\end{pmatrix}\begin{pmatrix}F & 1 & F\\ K' & \mp1 & -K\end{pmatrix}$$

That part of the Zeeman-operator, responsible for the off-diagonal terms, is given by;

$$2\mu_B\ B\ \left(\hat{S}^{BF}_{1}\ D^{1\ *}_{0\ 1}(\alpha,\beta,0) + \hat{S}^{BF}_{-1}\ D^{1\ *}_{0\ -1}(\alpha,\beta,0)\right)$$

The matrices (tables 2a & 2b) have been diagonalized. The parameter B_R and V_2 have been varied; the rotational constant B_r for O_2 (occurring in the expansion for $\epsilon^{(2)}$) was put equal to 43.1 GHz. The Zeeman- effect has been obtained comparing the eigenvalues for B=0 and B=2.81 Gauss. The linear dependence on B has been checked by a calculation for B=5.81 Gauss; the deviation from linearity was found smaller than 5 kHz, yielding a maximum relative effect of 0.2 percent, for the observed transition frequencies. The analytical approach reproduces the results of the numerical approach within 1 percent what concerns the energy levels in zero magnetic field and within 5 percent what concerns the Zeeman splitting, in a B-field of 2.81 Gauss.
In the following, the analytic approach is used to arrive at corrections of the intermolecular potential such that optimum agreement between observed and calculated Zeeman splittings is obtained.

tables 2a & 2b

p odd (table 2a)

	$\|2\rangle$	$\|3\rangle$	$\|4\rangle$
$\|2\rangle$	$\varepsilon_2 - \varepsilon_1$ $+B_R F(F+1)$ $+4\mu_B B \frac{M_F}{F(F+1)}$	$\mu_B B M_F \sqrt{\frac{2}{F(F+1)}} \sqrt{\frac{(F-1)(F+2)}{F(F+1)}}$ $-B_R \sqrt{2(F(F+1)-2)}$	
$\|3\rangle$	$\mu_B B M_F \sqrt{\frac{2}{F(F+1)}} \sqrt{\frac{(F-1)(F+2)}{F(F+1)}}$ $-B_R \sqrt{2(F(F+1)-2)}$	$\varepsilon_3 - \varepsilon_1$ $+B_R F(F+1)$	$\mu_B B M_F \sqrt{\frac{2}{F(F+1)}}$ $-B_R \sqrt{2F(F+1)}$
$\|4\rangle$		$\mu_B B M_F \sqrt{\frac{2}{F(F+1)}}$ $-B_R \sqrt{2F(F+1)}$	$\varepsilon_4 - \varepsilon_1$ $+B_R F(F+1)$

The energy matrices for the basis of the analytical approach, $|i;N,M_N;S,M_S;K,F,M_F\rangle$, where i indicates the involved ladder, N & M_N the quantum numbers of the O_2-rotation , S & M_S the spin quantum numbers of O_2, F the total angular momentum including the end-over-end rotation of the O_2Ar complex and K & M_F its projections. The projections described by M_N, M_S and K are taken along the body fixed dimer axis, that described by M_F along a space fixed direction defined by the time independent B-field. The off-diagonal terms derive from the Coriolis interaction and the Zeeman term. On the diagonal, in addition, the O_2-spin interactions (including higher order effects of M_N=0 & N>1-states) are taken into account (6). The two different energy matrices belong to even/odd parity states.

p even (table 2b)

	$\|1\rangle$	$\|2\rangle$	$\|3\rangle$
$\|1\rangle$	$B_R F(F+1)$		$\mu_B B M_F \sqrt{\frac{2}{F(F+1)}}$ $-B_R \sqrt{2F(F+1)}$
$\|2\rangle$		$\varepsilon_2 - \varepsilon_1$ $+B_R F(F+1)$ $+4\mu_B B \frac{M_F}{F(F+1)}$	$\mu_B B M_F \sqrt{\frac{2}{F(F+1)}} \sqrt{\frac{(F-1)(F+1)}{F(F+1)}}$ $-B_R \sqrt{2(F(F+1)-2)}$
$\|3\rangle$	$\mu_B B M_F \sqrt{\frac{2}{F(F+1)}}$ $-B_R \sqrt{2F(F+1)}$	$\mu_B B M_F \sqrt{\frac{2}{F(F+1)}} \sqrt{\frac{(F-1)(F+2)}{F(F+1)}}$ $-B_R \sqrt{2(F(F+1)-2)}$	$\varepsilon_3 - \varepsilon_1$ $+B_R F(F+1)$

For the direction of the r.f. B-field we choose the x-axis ($B_{dc}//z$). The magnetic dipole transition probability $|\imath\rangle \rightarrow |f\rangle$ is then proportional to $|\langle f|2\ \mu_B\ \hat{S}_x^{SF}|\imath\rangle|^2$ with (6)

$$\hat{S}_x^{SF} = \frac{1}{\sqrt{2}}\left(\hat{S}_{-1}^{SF} - \hat{S}_{+1}^{SF}\right) \quad \text{and} \quad \hat{S}_{\pm 1}^{SF} = \sum_{\nu} D^{1\ *}_{\pm 1,\nu}(\alpha,\beta,0)\ \hat{S}_{\nu}^{BF}$$

It is convenient to specify M_F and M_F', for the initial state $|\imath;M_F\rangle$ and the final state $|f;M_F'\rangle$ respectively. These kets are shorthand notations for $|\imath;M_F\rangle = |N,M_N;S,M_S;K,F;M_F\rangle$ and $|f;M_F'\rangle = |N,M_N';S,M_S';K',F;M_F'\rangle$
As we are dealing with Zeeman-transitions and use kets from the basis of the first order model, one has $M_N'=M_N$, $M_S'=M_S$, $K'=K$ and $F'=F$. By consequence , only $\nu=0$ contributes to the transition probability of Zeeman transitions. The relevant matrix-elements are

$$\langle f,M_F\pm 1|\ \sqrt{2}\ D^{1}_{\pm 1,0}(\alpha,\beta,0)\ \hat{S}_0^{BF}\ \mu_B|\imath,M_F\rangle =$$

$$\sqrt{2}\ \mu_B\ (-)^{-1+M_F-K}\ (2F+1)\begin{pmatrix} F & 1 & F \\ M_F\pm 1 & \mp 1 & -M_F \end{pmatrix}\begin{pmatrix} F & 1 & F \\ K & 0 & -K \end{pmatrix} M_S$$

This equation yields zero for $M_S=0$ (ladder 3 of ref. 6) and for $K=0$ (ladder 1 and 4 of ref. 6). Thus, only the Zeeman splitting of ladder 2 ($|K|=2$, $|M_S|=1$) contributes to the Zeeman spectrum.
Using again the representation with definite parity (table 1 of ref. 6) one obtains for the squared transition matrix element

$$P_{F,M_F}(\text{ladder 2}) = \mu_B^2(2F+1)^2\left[\begin{pmatrix} F & 1 & F \\ M_F-1 & 1 & -M_F \end{pmatrix}^2 + \begin{pmatrix} F & 1 & F \\ M_F+1 & -1 & -M_F \end{pmatrix}^2\right]\begin{pmatrix} F & 1 & F \\ -2 & 0 & 2 \end{pmatrix}^2$$

Here, transitions which increase and decrease M_F, have been taken into account. To compare to the relative experimental transition probability (at low r.f. fields) one has to sum this last expression over M_F,

$$P_F(\text{ladder 2}) = \frac{8}{F(F+1)}\,\mu_B^2$$

So far it has been assumed that the mixing of the first order eigenstates which is produced by diagonalisation of the matrices (tables 2a & 2b) has negligible influence on the transition probabilities. From the calculated mixing amplitudes we estimate that the forbidden transitions within the first, third and fourth ladder become allowed but obtain a strength at least ten times smaller than that for the second ladder. The reason for this simplifying circumstance resides in the fact that the operator $2\mu_B \hat{S}_x^{SF}$ possesses no off-diagonal elements between states from different i-ladders.

In comparison, the transition probability for O_2 monomers amounts to

$$P_J(O_2) = \frac{1}{J(J+J)}\,\mu_B^2\,\Big[2 + J(J+1) - N(N+1)\Big]^2$$

In the experimental results (fig. 4) two double peaks and three single peaks can be distinguished. Note , that the experimental FWHM line width amounts to about 50 kHz. One observes also spectral structures below 750 kHz, for B=2.81 Gauss.

In the same figure the positions of the Zeeman splitting due to the potential model (10) are indicated, as calculated within the numerical approach (4). The two double peaks have been assigned to F=2+,- and F=3+,- with splitting <50 kHz and the three single peaks to F=4+, F=4- and F=5-. The levels contributing to the structure below 750 kHz are indicated. The narrow peak at about 380 kHz (8-, 14+ and 15- levels) appears slightly stronger than expected from a simple extrapolation of intensity from the well assigned higher frequency peaks. We have considered and finally rejected the possibility that there is some contribution from ladder 3, due to strong mixing between wave functions of ladder 2 and 3, at high F-values. The Zeeman splitting of the levels F=19+, 18-, 17+, 16-, 15+ and 14- comes close to the observed maximum. However, the Boltzmann factor for these high levels of ladder 3 renders this hypothesis rather unprobable (we have assumed T=3 K). Another hypothesis is equally rejected. From the numerical (table 1) and analytical approach we know that the levels of ladder 1 posses a Zeeman splitting with a maximum value (about 400 GHz) at around F=11, i.e. F=7+, 8-, ..., 15+ and 16- all contribute at about the same frequency, (380 GHz). Here, however, the expected small transition probability rules out this conjecture.

Although the agreement is rather good, the Zeeman splittings predicted by the numerical model (fig. 4) do not exactly reproduce the experimental positions. This is due to inaccuracy of the empirical potential (10). In order to obtain

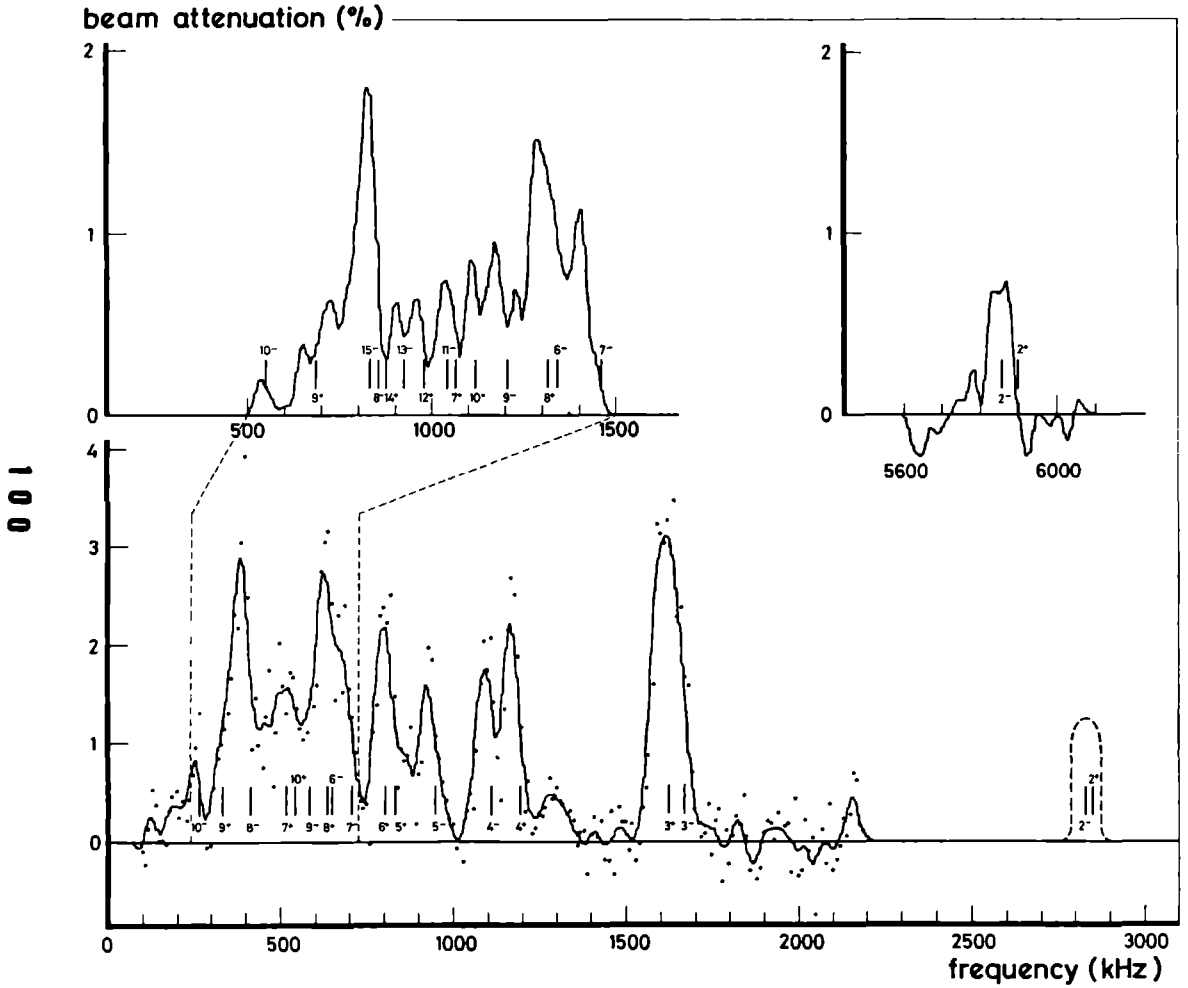

figure 4. The Zeeman spectrum of O_2Ar, measured as beam attenuation (percentage) versus rf transition frequencies. The lower trace is recorded at B=2.81 Gauss, the left and right upper trace at B=5.81 Gauss. The experimental uncertainty is smaller than 0.13 percent. Zeeman splittings from the numerical approach are assigned and indicated by bars, according to the potential model (10). The broken line indicates the position of the F=2+,- splitting inferred from the measurement at 5.81 Gauss.

an even better agreement we use the analytical model to correct for small changes in the potential, see fig. 5. Although the absolute values for the Zeeman splittings are 5 percent too high as obtained from the analytical approach we assume that small relative shifts are produced with sufficient accuracy by a variation of the parameters V_2 and B_R. At B=2.81 Gauss, V_2=1150 GHz and B_R=2.07 GHz an increase of V_2 by 25 GHz yields an average shift of the Zeeman splitting of 1.5±0.2 kHz, to lower frequencies. Under the same conditions, an increase of B_R by 0.1 GHz yields an average shift of the Zeeman splitting of 13±4 kHz, to higher frequencies. The corresponding shifts for B=2.81 Gauss at V_2=800 GHz and B_R=2.07 GHz are 2.2±0.4 kHz and 13±4 kHz, respectively. Fortunately, there is no strong dependence on the starting values for V_2 and B_R. Note that the actual shifts were obtained by using the explicit dependence of all Zeeman splittings on the parameters V_2 and B_R, for each individual low lying level of ladder 2, for the various parameter combinations of fig. 6.

Our starting values, V_2=1150 and B_R=2.07 GHz (combination 1, left dot in fig. 6) are calculated from the numerical approach, taking expectation values of $V_2(R)$ and $(2\mu R^2)^{-1}$ between the "exact" eigenfunctions of (4). As mentioned above, there is only a weak dependence on the particular choice of eigenfunctions for neighbouring low-lying states.

The V_2 and B_R parameters are not independent. For decreasing R-values both V_2 and B_R rise, for instance to B_R=2.13 GHz and V_2=2300 GHz (combination 2, right dot in fig. 6); this combination is obtained from an "exact" numerical solution of the ro-vibration-spin problem with the V_2-potential shifted to higher R-values by 0.12 Å. In fig. 6, those combinations are indicated, which fall onto the linear interpolation between combination 1 and 2. At the same time, for various V_2-B_R combinations

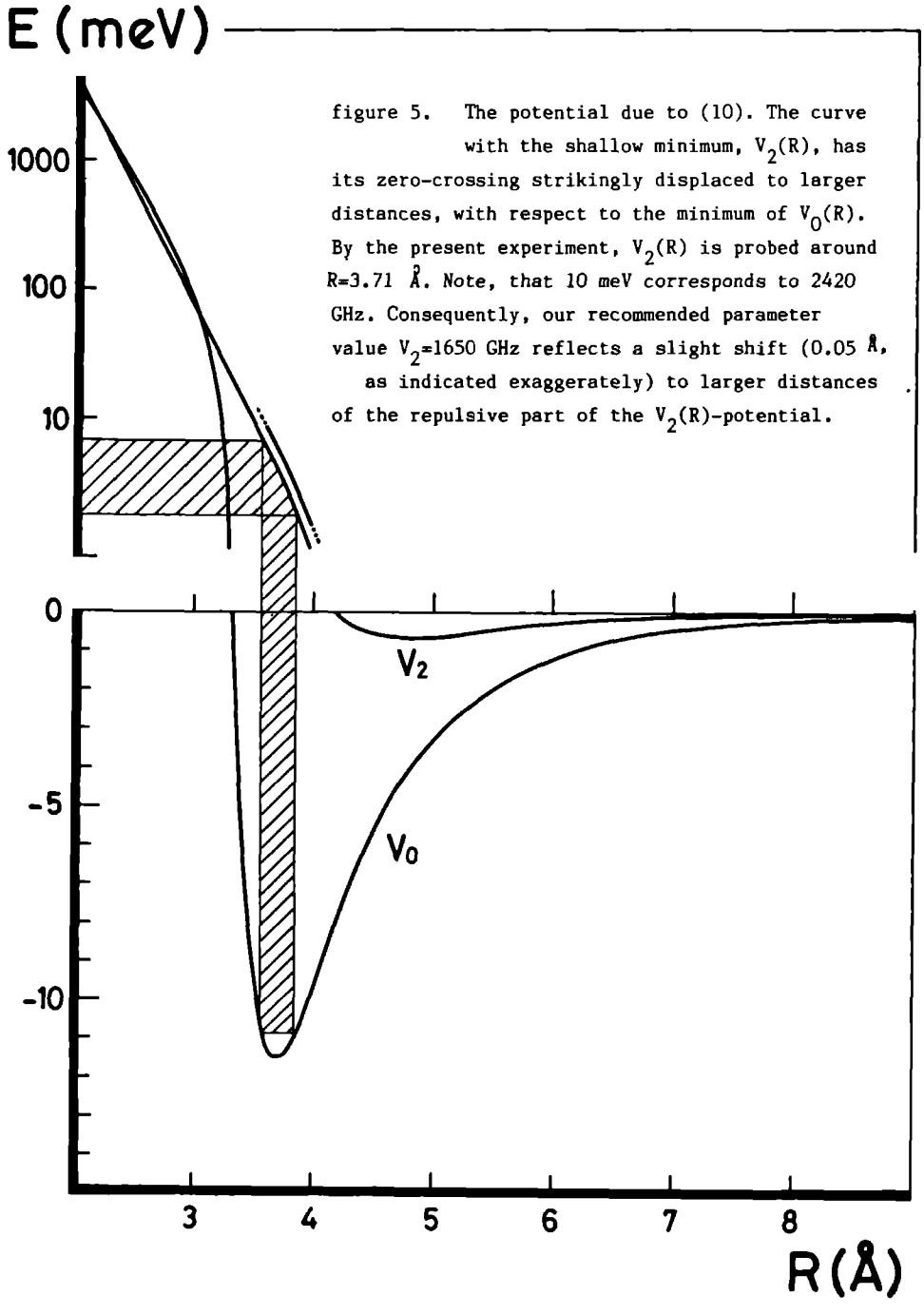

figure 5. The potential due to (10). The curve with the shallow minimum, $V_2(R)$, has its zero-crossing strikingly displaced to larger distances, with respect to the minimum of $V_0(R)$. By the present experiment, $V_2(R)$ is probed around R=3.71 Å. Note, that 10 meV corresponds to 2420 GHz. Consequently, our recommended parameter value V_2=1650 GHz reflects a slight shift (0.05 Å, as indicated exaggerately) to larger distances of the repulsive part of the $V_2(R)$-potential.

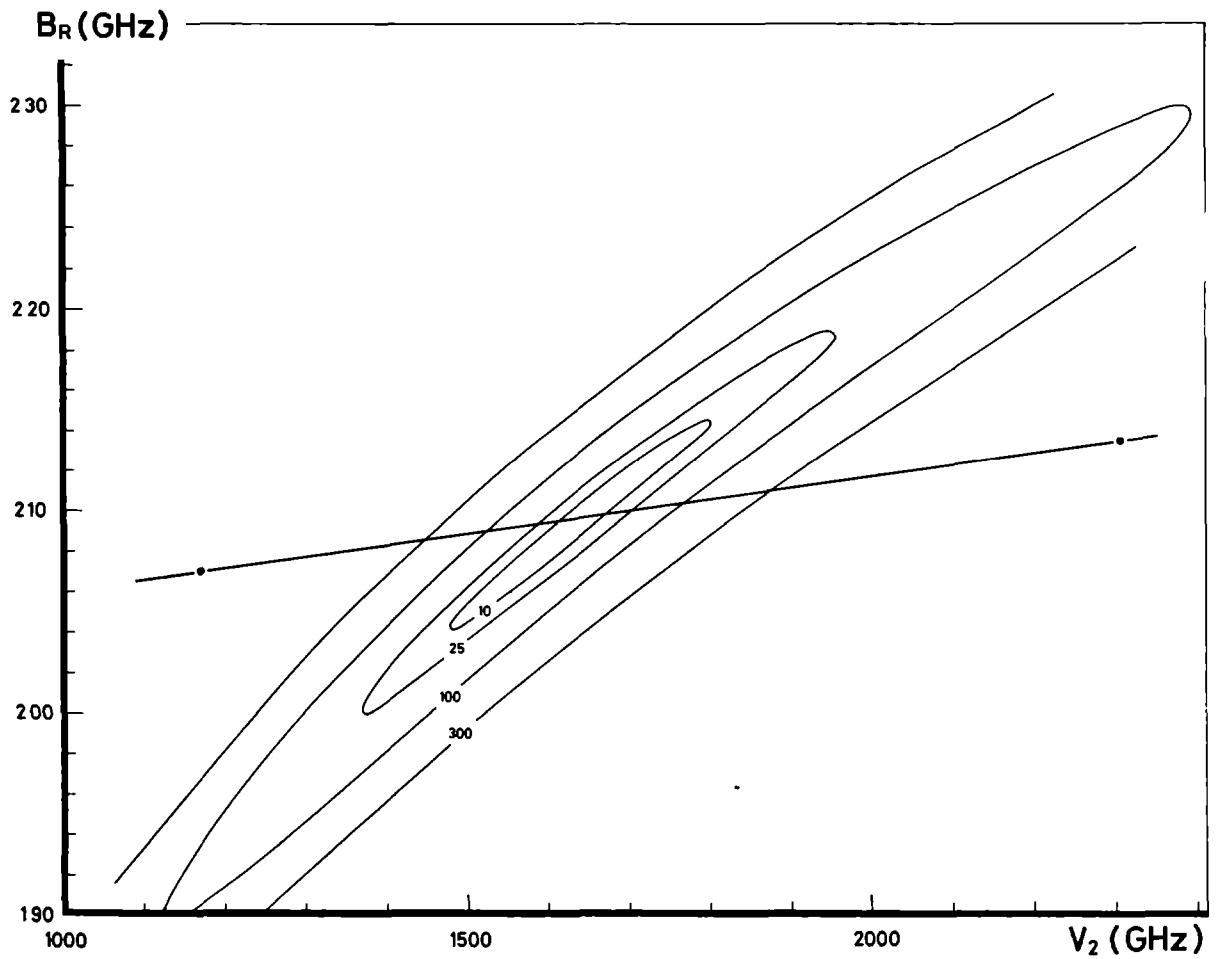

figure 6. The optimum valley of the B_R-V_2-parameters from the analytical approach. The number along the curves represent Δ^2 in $(kHz)^2$, the sum over the squared differences between the measured and calculated Zeeman splittings. As characterisation of our experimental uncertainty we take Δ^2=100. The left dot corresponds to the B_R-V_2 combination 1, obtained with the help of the exact eigenfunctions belonging to the potential of (10). The right dot is calculated similarly, after a 0.12 Å shift of $V_2(R) \rightarrow V_2(R-0.12)$. Between these dots, the linearly interpolated line describes the correlation between B_R and V_2; its intersection with the optimum valley yields our recommended values.

the sum of squared differences between the measured and calculated Zeeman splitting, Δ^2, is shown for the F<5+ levels of ladder 2. The intersection of the linear interpolation of combinations 1 & 2 with the valley of $\Delta^2 \leq 100$ $(kHz)^2$ yields the recommended V_2 & B_R values, from our experiment.

The conclusions of this paper are summarized in the following statements; the T-shaped dimer O_2-Ar can be well understood and described by a simple model (6); the predictions of this model are satisfactorily verified by our experiments on the Zeeman splitting; the potential model of Pirani & Vecchiocattivi (10) needs only slight adjustment, in the light of the present experiment; the optimum parameter-values we propose are V_2=1650±125 GHz and B_R=2.097±0.007 GHz, corresponding to a shift of 0.05 Å to larger intermolecular distances, of the repulsive branch of $V_2(R)$ (see fig. 5).

ACKNOWLEDGEMENT

We would like to thank L. Meerts for the EBR excursion and G. Brocks for the revival of the numerical program and the additional calculation of combination 1 and 2 of figure 6.

The authors are grateful for the technical support received at Nijmegen from messrs. J. Holtkamp, F. van Rijn, C. Sikkens and L. Hendriks for skilful assistance.

Finally acknowledgement is made of the financial support of NATO in the provision of a travel grant (grant no. 139.80) for one of us (Derek Lainé), and the Stichting voor Fundamenteel Onderzoek der Materie (FOM) for supporting this project financially.

LIST OF REFERENCES

ref 1 A. Amirav, U. Even and J. Jortner
J. Chem. Phys. 73 (1980) 4217

ref 2 W.L. Meerts, private communication.

ref 3 W.L. Meerts and I. Ozier, to be published Can. J. of Phys.

ref 4 J. Tennyson and J. Mettes
Chem. Phys 76(1983) 195.

ref 5 J. Mettes, B. Heijmen, D.C. Laine and J. Reuss
Method to determine the rotational temperature in a molecular beam, demonstrated on O_2, accepted Chem. Phys.

ref 6 A. van der Avoird
J. Chem. Phys. 79(1983) 1170

ref 7 N. F. Ramsey, molecular beams (Oxford University Press, 1956)

ref 8 M.Mizushima,
The theory of rotating diatomic molecules (Wiley, New York, 1975)

ref 9 D. M. Brink and G.R. Satchler,
Angular momentum (Clarendon Press, Oxford, 1968)

ref 10 F. Pirani and F. Vecchiocattivi, Chem. Phys. 59 (1981) 387

ref 11 G. Henderson and G. Ewing, J. Chem. Phys. 59 (1973) 2280

O_2Ar being measured and understood the question poses itself what can and shall be done next, with the Nijmegen magnetic beam resonance machine, utilizing the improvements achieved during the period of this thesis work.

Naturally, O_2-Ne and simular combinations offer themselves as candidates for extended studies. New aspects are encountered if $(O_2)_2$ is considered where intermolecular spin-spin forces come into play providing us with possibly new magnetic effects; indeed, in the course of our work we have encountered evidence, that $(O_2)_2$ becomes diamagnetic below about 10 K. This is new because one has expected - partially based on the work of van Deursen and in contrast to what is known for $(NO)_2$ - that $(O_2)_2$ remains paramagnetic. However, very recently the group of Van der Avoird questioned this belief by demonstrating theoretically, that for most geometries, $(O_2)_2$ becomes a diamagnetic complex.

Before we set out to investigate paramagnetic molecules and paramagnetic clusters, a test measurement was performed to show the feasibility of magnetic beam resonance measurements on diamagnetic molecules as heavy as SF_6. The positive outcome has opened the way to measurements where intersection of the molecular beam e.g. by a properly tuned CO_2-laser permits to select rf magnetic beam resonance signals for well defined rotational states.

Another possibility of the application of ir laser in conjunction with MBR might be the investigation of hydrogen bonded dimers, in a non- destructive way; excitation becomes observable by the change of magnetic deflection upon vibrational transition, e.g. for $(NH_3)_2$. The gain in spectral

resolution - as compared to predissocation studies - could be considerable.

All these and other possibilities have to be looked at in the light of the achieved technical progress. We are convinced to have gained 1 à 2 orders of magnitude in sensitivity - otherwise a single-state measurement of a 10^{-5} - cluster fraction would not have been possible. With this achievement it looks worthwhile to go back to formerly unsuccesful attempts. Especially, the hfs-determination of $(H_2)_3$ we would have liked to try again, employing noise broadening to facilitate the initial search of resonance frequencies. However, the life-time of an average dutch promovendus is finite; besides, a savory menu should be left to my successor!

Het T-vormige dimeer O_2-Ar kan met behulp van een simpel model beschreven en begrepen worden: de voorspellingen van dit model worden op een bevredigende manier bevestigd door onze metingen aan de Zeeman splitsing, het potentiaal model van Pirani & Vecchiocattivi heeft slechts een kleine verandering nodig in het licht van het gepresenteerde experiment, de door ons gepresenteerde optimale waarden van de parameters zijn V_2=1650±125 GHz en B_R=2.097±0.007 GHz, wat neerkomt op een verschuiving van het repulsieve stuk van $V_2(R)$ van 0.05 Å naar een grotere intermoleculaire afstand.

Curriculum Vitae

Ik ben geboren op 21 mei 1951 te Nijmegen.
Op 4 juni 1969 behaalde ik het diploma HBS b. In september 1974 ben ik aan mijn studie natuurkunde aan de universiteit te Nijmegen begonnen, dit resulteerde in het kandidaats-examen op 10 november 1977. Op 11 december 1980 behaalde ik het doctoraal-examen, na een stage-periode op de afdeling atoom- en molecuulfysica van professor Reuss.
Deze laatste bood mij een promotiebaan aan die vrijkwam in juni 1981,die ik heb geaccepteerd.

STELLINGEN

1 In tegenstelling tot de bevindingen van A. Van Deursen wijst alles erop dat de grondtoestand van $(O_2)_2$ diamagnetisch is.

zie A. Van Deursen and J. Reuss, Molecular beam intensities and collision cross-sections of small Ne, H_2, N_2, NO and O_2 clusters.

2 De detectie limiet van kleine gasconcentraties gemeten in een opto-acoustische cel wordt vaak bepaald door een achtergrond signaal (1).

1/ R. D. Kamm, Detection of weakly absorbing gases using a resonant opto-acoustic method. J. of Appl. Phys. 47 (1976) 3550.

3 Scheiding van de zuurstof moleculen $O^{16}O^{16}$ en $O^{16}O^{18}$ in een bundel beschreven in (1), waarbij gebruik wordt gemaakt van isotoop selectieve resonantie kan in dit specifieke geval veel efficienter worden verricht door gebruik te maken van het feit dat $O^{16}O^{18}$ een paramagnetische grondtoestand heeft en $O^{16}O^{16}$ niet, dit in combinatie met een voldoende koude bundel.

1/ A. Amirav and U. Even, J. Appl. Phys. 51 (1980) 1.

4 De formule voor $E_{rot}(J=N-1)$ van een $^3\Sigma$ state (1) uit Mizushima's " The Theory of Rotating Diatomic Molecules " geeft voor $O^{16}O^{16}$, met de constanten genomen uit tabel (2) uit hetzelfde boek, een verkeerde waarde, voor N=1.

1/ tabel 5-1 blz 229.
2/ tabel 5-4 blz 238.

5 Omdat in principe alle twee-foton-excitaties, binnen een infrarood aktieve mode, Raman aktief zijn, kun je via Raman-metingen van boventonen & combinatie tonen belangrijke informatie verkrijgen ter interpretatie van multiphoton dissociatie-spectra & -processen.

zie E. Borsella, R. Fantoni, A. Giardini-Guidoni, D. R. Adams and C. D. Cantrell, Resonance structure of multiple-photon excitation in symmetric and asymmetric tops, Chem. Phys. Letters 101 (1983) 86.

6 De extreem grote rotatie constante van SiH_4 (nl. 2.85 cm^{-1}) zou het mogelijk moeten maken om met een continu verstembare TEA laser en een meetopstelling zoals in (1) rotatie opgeloste spectra te verkrijgen en zo de weg te volgen van multiphoton processen zoals beschreven in (2).

1/ E. Borsella, R. Fantoni, A. Giardini-guidoni, D. R. Adams and C. D. Cantrell, Resonance structure of multiple-photon excitation in symmetric and asymmetric tops, 101 (1983) 86.

2/ W. Fuss, Comments on collisionless vibrational relaxation, Chem. Phys. 76 (1983) 343-348.

7 Het aanbrengen van afbeeldingen bij in het nederlands opgestelde tekst van de te bestellen artikelen van instellingen zoals de fakulteits kantine wis- & natuurkunde te Nijmegen zou ook voor buitenlandse gasten de mogelijkheid openen om een bewuste keuze te maken.

bron: Dr. Lainé, die herhaaldelijk, ontdanks lang oefenen op de uitspraak van "vruchtensla", genoegen heeft moeten nemen met yoghurt.

8 De indruk dat de pessimist vaak gelijk heeft wordt ten onrechte versterkt doordat enerzijds - als er inderdaad iets mis is gegaan - hij er vaak melding van maakt dat hij dit al had zien aankomen, èn anderzijds - als het toch goed is gegaan - hij verzuimt terug te komen op zijn voorspelling, iets dat dikwijls in de roes van de vroegde over de goede afloop aan de betrokkenen niet opvalt.